Dissertation zur Erlangung des Doktorgrades

der Fakultät für Chemie und Pharmazie

der Ludwig-Maximilians-Universität München

Artificial Angiogenesis

-

Characterization of endothelial cell migration in three-dimensional model systems

Kerstin Kick, geb. Pflieger

aus

Deggendorf, Deutschland

2015

Erklärung

Diese Dissertation wurde im Sinne von §7 der Promotionsordnung vom 28. November 2011 von Herrn Prof. Dr. Stefan Zahler betreut.

Eidesstattliche Versicherung

Diese Dissertation wurde eigenständig und ohne unerlaubte Hilfe erarbeitet.

München, den 01.03.2016

Kerstin Kick

Dissertation eingereicht am:	14.12.2015
1. Gutachter:	Prof. Dr. Stefan Zahler
2. Gutachter:	Prof. Dr. Angelika M. Vollmar
Mündliche Prüfung am:	17.02.2016

Meinem Ehemann

CONTENTS

CONTENTS

CONTENTS I

ABBREVIATIONS IV

TABLES VI

FIGURES VII

1 INTRODUCTION 2
1.1 Neovascularisation 2
1.1.1 Vasculogenesis 2
1.1.2 Angiogenesis 2
1.2 Endothelial cells 3
1.2.1 Diversity and function of endothelial cells 3
1.2.2 Tip and stalk cell characteristics 4
1.3 Cell migration 5
1.3.1 Three dimensional cell migration 5
1.3.2 Rho GTPase signalling in cell migration 6
1.4 Artificial angiogenesis 8
1.5 Tube formation 8
1.6 Hydrogels 8
1.7 Aim of the study 10

2 MATERIAL AND METHODS 12
2.1 Material 12
2.2 Methods 12
2.2.1 Cell culture 12
2.2.2 Hydrogels 13
2.2.3 Retina preparation and imaging 13
2.2.4 Rheology of hydrogels 15
2.2.5 Immunostainings 15
2.2.6 Single cell migration 16
2.2.7 Tube formation assay 17
2.2.8 Polyacrylamide gels coated with Matrigel 18
2.2.9 Traction force microscopy 19
2.2.10 Microfluidics 19
2.2.11 Statistical evaluation 20

3 RESULTS 22
3.1 Spatio-temporal characterization of endothelial tube formation 22
3.1.1 Formation of cell-cell contacts depends on the mean distance between single cells 22
3.1.2 Morphogenesis is not based on soluble or matrix bound gradients of growth factors 24
3.1.3 Cells actively deform their substrate to attract other cells 27

3.1.4 Endothelial tube formation with different cell-to-cell distances depends on the rigidity of the matrix 29
3.1.5 Proteolytic activity is not essential for the formation of tubes 30
3.1.6 Cell adhesion to laminin is essential for endothelial tube formation 30
3.1.7 Contractility impacts endothelial tube formation 31
3.1.8 Simulation of endothelial tube formation shows a directed, force dependent process 32
3.2 Comparative characterization of single endothelial cell migration in Matrigel and collagen I gels 33
3.2.1 Matrix composition influences morphology of migrating endothelial cells 33
3.2.2 The role of myosin II-dependent contractility depends on matrix composition 36
3.2.3 Matrix composition influences polarization of small GTPases in endothelial cells 38
3.2.4 Self-secreted ECM proteins are deposited during migration in Matrigel and *in vivo* 40
3.2.5 Cell blebbing compensates for loss of proteolytic activity in collagen I gels 42
3.2.6 Inhibition of laminin binding integrins induces a morphological switch of endothelial cells 44
3.2.7 Endothelial cell migration *in vivo* approves elongated migration morphology, inhibition of laminin binding induces a morphological switch 46

4 DISCUSSION 49
4.1 Mechanical forces exerted on the matrix and matrix adhesion are decisive for endothelial tube formation 49
4.1.1 Formation of initial cell-cell contacts is a directed process dependent on cell density 49
4.1.2 VEGF gradients are not inevitable for communication of cells 50
4.1.3 Initial communication of cells depends on mechanical forces exerted on the substrate 50
4.1.4 Laminin binding integrins might act as force sensors 51
4.1.5 Cell adhesion and thus morphology of endothelial cells plays a pivotal role for the maturation of tubular structures 52
4.2 Endothelial cells switch their migration modes based on matrix composition 53
4.2.1 Matrix topography influences endothelial cell morphology 53
4.2.2 Bleb-driven migration in rat tail collagen I depends on contractility and polarization of small GTPases 53
4.2.3 Physiological remodeling of the ECM is absent in collagen I gels 54
4.2.4 Laminin determines the migration mode 55
4.2.5 Physiological migration of endothelial cells in mouse retina is similar to elongated migration morphology in Matrigel 55
4.3 Conclusion and future perspectives 56

5 SUMMARY 58

6 REFERENCES 61

7 APPENDIX 72
7.1 Material 72
7.1.1 General equipment and chemicals 72
7.1.2 Microscope equipment and consumables 73
7.1.3 Cell culture consumables 74
7.1.4 Inhibitors 74
7.1.5 Antibodies for immunofluorescence 75
7.1.6 Fluorescent dyes 75
7.1.7 Hydrogels 75
7.1.8 Buffers 76
7.2 Simulation parameters 77
7.3 Publications 78
7.3.1 Original publications 78
7.3.2 Poster presentations 79
7.3.3 Oral presentations 79
7.4 Curriculum Vitae 80
7.5 Danksagung 81

ABBREVIATIONS

µg	Microgram
µl	Microliter
µm	Micrometer
µNm	Micronewton meter
2D	Two-dimensional
3D	Three-dimensional
APS	Ammonium persulfate
APTES	(3-aminopropyl) trimethoxysilane
BSA	Bovine serum albumin
CCD	Charge coupled device
Cdc42	Cell division control protein 42
cm	Centimeter
DDS	Dichlordimethylsilane
Dll4	Delta-like ligand 4
DMSO	Dimethyl sulfoxide
DNA	Deoxyribonucleic acid
EC	Endothelial cell
ECBM	Endothelial cell basal medium
ECGM	Endothelial cell growth medium
ECM	Extracellular matrix
EGFP	Enhanced green fluorescent protein
f-actin	Filamentous actin
FCS	Fetal calf serum
FMI	Forward migration index
GDP	Guanosine diphosphate
GTP	Guanosine triphosphate
HUVEC	Human umbilical vein endothelial cells
Hz	Hertz
l	Liter
M	Molarity
mAb	Monoclonal antibody
MCS	Monte Carlo step
mg	Milligram
ml	Milliliter
MLC	Myosin light chain
mm	Millimeter
MMP	Matrixmetalloproteinase
nm	Nanometer
Nrp 1	Neuropilin-1
P3	Postnatal day three
Pa	Pascal
PAA	Polyacrylamide
pAb	Polyclonal antibody

PBS	Phosphate buffered saline
PFA	Para-formaldehyde
Rac1	Ras-related C3 botulinum toxin substrate 1
ROCK	Rho-associated protein kinase
rpm	Revolutions per minute
rps	Revolutions per second
TEMED	Tetramethylethylenediamine
U	Unit
UV	Ultraviolet
VEGF	Vascular endothelial growth factor
VEGFR	Vascular endothelial growth factor receptor

TABLES

Table 1 General lab equipment and consumables 72
Table 2 Chemicals 72
Table 3 Microscope equipment and consumables 73
Table 4 Cell culture consumables 74
Table 5 Pharmacological inhibitors 74
Table 6 Primary and secondary antibodies 75
Table 7 Fluorescent dyes 75
Table 8 Natural hydrogels 75
Table 9 Buffers 76
Table 10 Parameters for simulation of endothelial tube formation 77

FIGURES

Figure 1 Steps of vessel sprouting during angiogenesis 3
Figure 2 Tip and stalk cell specification during sprouting angiogenesis 5
Figure 3 Signalling in lamellipodia 7
Figure 4 Rho GTPases in bleb-driven migration 7
Figure 5 Illustration of the microfluidic experiment 20
Figure 6 A minimum cell density is required for network assembly 23
Figure 7 Relative motion of the cell population is a directed process 24
Figure 8 Neither bound nor soluble gradients are critical for EC tube formation 26
Figure 9 HUVECs exert forces on the ECM 28
Figure 10 Matrix stiffness influences endothelial tube formation 29
Figure 11 HUVEC tube formation is not hindered by inhibition of MMPs 30
Figure 12 Adhesion to laminin is crucial for endothelial tube formation 31
Figure 13 Inhibition of contractility hinders endothelial tube formation 32
Figure 14 Simulation of the endothelial tube formation process shows a directed, force-dependent migration 33
Figure 15 Substrate topography influences morphology of ECs 35
Figure 16 Morphological and functional characterization of ECs in Matrigel and collagen I 37
Figure 17 Rac1 and Cdc42 as key-players in migration show different polarization-dependent effects in Matrigel and collagen I 39
Figure 18 ECs deposit ECM-proteins in Matrigel and in mouse retina tissue but not in collagen I gels 41
Figure 19 Different effects of MMP inhibition in Matrigel and in collagen I gels 43
Figure 20 Laminin determines elongated migration mode 45
Figure 21 Live-imaging of ECs in mouse retina shows elongated mode of migration *in vivo* 47
Figure 22 Summary of the thesis 59

1 INTRODUCTION

1 INTRODUCTION

1.1 Neovascularisation

Vasculogenesis and angiogenesis are the fundamental processes, forming new blood vessels[1].

1.1.1 Vasculogenesis

During vasculogenesis, endothelial cells (ECs) derive from the successive differentiation of mesodermal cells into hemangioblasts, which leads to the formation of the first vascular structures. The hemangioblasts from the centre of primitive blood islands give rise to the hematopoietic stem cells, whereas the peripheral hemangioblasts differentiate into angioblasts, the precursors of mature ECs[2]. Under the influence of vascular endothelial growth factor (VEGF), the angioblasts and newly formed ECs migrate on a matrix constituted mainly of collagen and hyaluronan, allowing the fusion of blood islands, their remodelling into tubular structures, and the formation of the first vascular plexus. These tubules remodel through vasculogenesis into larger vessels, leading to vascularization of the embryo[3].

1.1.2 Angiogenesis

In contrast to vasculogenesis, angiogenesis refers to the formation of blood vessels from pre-existing ones. Two distinct mechanisms of angiogenesis have been described: sprouting and intussusception. Intussusceptive angiogenesis is caused by the insertion of interstitial cellular columns into the lumen of pre-existing vessels and the subsequent stabilization results in partitioning of the vessels and remodelling of the local vascular network[4]. Sprouting angiogenesis entails two successive phases: neovessel growth and neovessel stabilization.

Angiogenesis is required in many physiological and pathological processes, including embryonic development, wound healing, tissue regeneration, and the growth and metastasis of solid tumors[5]. Attracted by proangiogenic signals, ECs become motile and invasive and protrude filopodia. These so-called tip cells lead new sprouts and probe the environment for guidance cues. Following tip cells, stalk cells proliferate to support sprout elongation. Tip cells fuse with cells from neighbouring sprouts to build vessel loops

(Figure 1). The initiation of blood flow, the establishment of a basement membrane, and the recruitment of mural cells stabilizes new connections[6]. This sprouting process iterates until proangiogenic signals are reduced.

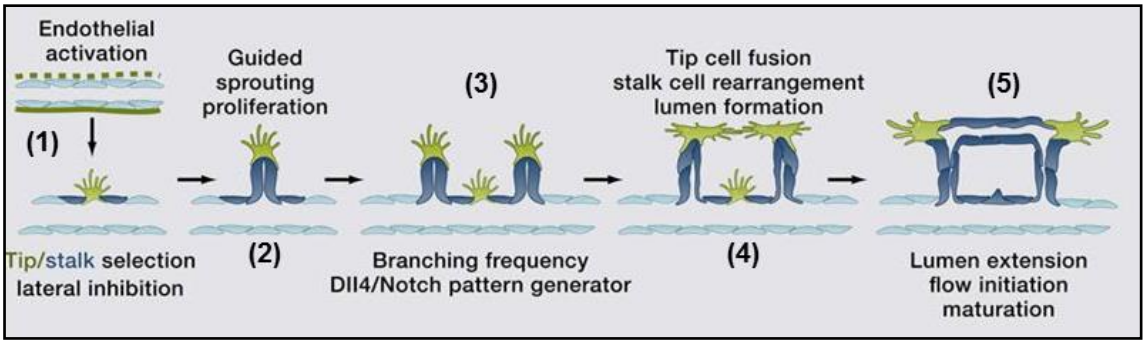

Figure 1 **Steps of vessel sprouting during angiogenesis**. (1) Tip/stalk cell selection; (2) tip cell navigation and stalk cell proliferation; (3) branching coordination; (4) stalk cell elongation, tip cell fusion, and lumen formation; (5) perfusion and vessel maturation (adapted from *Potente et al.*[6]).

1.2 Endothelial cells

1.2.1 Diversity and function of endothelial cells

In adults, most ECs are quiescent and poised for repair. Whilst it was originally thought that all ECs were homogenous[7], it is now commonly accepted that there is a high degree of heterogeneity along the vascular tree, to allow biological adaption to local needs[8]. The structural and functional diversity of ECs has been investigated between different EC populations including arteries and veins[9], large and small vessels[10] and normal and tumor vessels[11]. This diversity is the result of molecular differences between EC populations.

During angiogenesis, ECs perform a variety of functions, including degradation of the extracellular matrix (ECM), migration, proliferation, lumen formation, and vessel stabilization. Roles for the Rho GTPases RhoA, Cdc42, and Rac1 have been identified in many of these processes[12].

The most commonly used human ECs for *in vitro* angiogenesis assays are human umbilical vein endothelial cells (HUVECs), which are isolated by perfusion of the umbilical vein with trypsin or collagenase and have been successfully cultured since 1973[13].

1.2.2 Tip and stalk cell characteristics

The first cell in a vessel branch is the tip cell, which leads the way[14]. Key features of this cells are their location at the forefront of vessel branches, highly polarized nature, and numerous filopodia probing the environment, while migrating toward an angiogenic stimulus. Tip cells do not form a lumen and mostly proliferate minimally[15]. They have a specific molecular signature, characterized by the expression of vascular endothelial growth factor receptor (VEGFR) 2, VEGFR3, platelet-derived growth factor (PDGF), Delta-like ligand 4 (Dll4) and others[16–18]. These cells detect gradients of navigator cues and integrate combinatorial molecular codes into directional migration[14]. A second endothelial subtype is called stalk cell. This cell trails behind the leading tip cell and tasks at proliferation, stalk elongation, lumen formation and connection to the circulation[19]. In contrast to tip cells, stalk cells do not form filopodia[15].

VEGF and Notch signalling pathways are key players governing tip and stalk cell behaviour (Figure 2): VEGF interacts with VEGFR2, expressed at the surface of ECs of quiescent vessels. Neuropilin-1 (Nrp1) modulates the VEGF signalling output, enhancing the binding activity and signalling of VEGF through VEGFR2. Under VEGF stimulation, Dll4 expression is up-regulated in the tip cells. In turn, Dll4 ligand activates Notch signalling in the stalk cells, consequently suppressing the tip cell phenotype. Notch signalling activation reduces VEGFR2 expression and increases VEGFR1 levels as well as the expression of different Notch target genes. In contrast, the tip cell receives low Notch signalling, allowing high expression of VEGFR2 and Nrp1, but low VEGFR1. Contrary to Dll4, Jagged1 ligand is expressed by stalk cells. Jagged1 antagonizes Dll4/Notch signalling in the sprouting front when the Notch receptor is modified by Fringe. The duration and amplitude of the Notch signal are modulated by Sirtuin-1 (SIRT1), which primes the Notch intracellular domain for ubiquitination and degradation by direct acetylation[20].

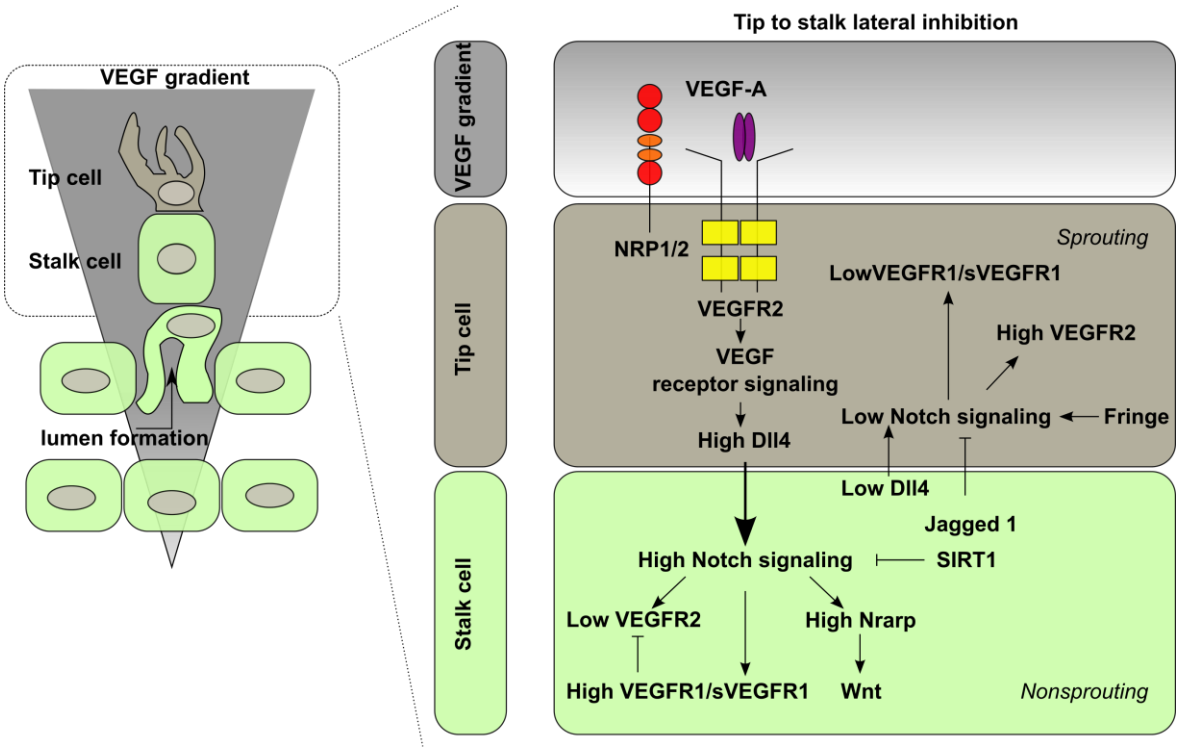

Figure 2 **Tip and stalk cell specification during sprouting angiogenesis.** During vascular angiogenesis, VEGF and Notch signalling pathways are implicated in the specification of the tip and stalk cells in the vascular endothelium (adapted from Blanco *et al.*[20]).

1.3 Cell migration

1.3.1 Three dimensional cell migration

The basic concepts underlying EC migration have been obtained mostly from observations in two-dimensional (2D) cell culture systems[2,5]. However, the three-dimensional (3D) environment encountered *in vivo* is far more complex. The cells have to integrate and coordinate their adhesion with the ECM and interpret attractive and repulsive cues to choose their path[21,22].

Many studies in the last years revealed that different cell types employ different mechanisms to migrate into and navigate through the ECM. Studies in primary human fibroblasts showed that structurally distinct 3D environments support different modes of cell migration, and that polarization of phosphatidylinositol (3,4,5)-triphosphate (PIP3) and Rho family GTPase signaling differs between lobopodia- and lamellipodia-based 3D migration[23]. Studies of leukocyte motility and cancer cell migration in 3D environments revealed a switch of these cells between adhesion-dependent mesenchymal (elongated) and adhesion-independent amoeboid (rounded) cell motility. This motility is driven by actin

polymerization, and actomyosin contraction[24,25]. Actomyosin dynamics appeared to constitute a core component of bleb formation. Plasma membrane blebbing was primarily viewed as a by-product of apoptotic and necrotic processes[26]. However, subsequent studies could show that cell blebbing is not limited to the execution of cell death programs[27,28], but is also implicated in cell movement. Actually, plasma membrane blebs are now numbered among other cell migration mediating protrusions like filopodia, lamellipodia, invadopodia, and podosomes[29].

1.3.2 Rho GTPase signalling in cell migration

What is common to all the above mentioned modes of migration is the involvement of Rho GTPases. There are 20 Rho GTPase genes in humans[30]. Most Rho GTPases are active and stimulate their downstream targets when bound to guanosine triphosphate (GTP), and inactive when bound to guanosine diphosphate (GDP). They are activated by guanine nucleotype exchange factors (GEFs), which induce the exchange of GDP for GTP, and inactivated by GTPase-activating proteins (GAPs), which catalyse the hydrolysis of GTP to GDP. The best studied Rho GTPases are Rho, Rac and Cdc42[31].

In 3D environments, slow moving cells, such as fibroblasts can extend lamellipodia[23], which have been frequently observed at the front of single cells, as well as at the leading front of collectively migrating cells[32,33]. Under normal conditions, lamellipodium-driven migration requires active Rac proteins, interacting with a WAVE-associated complex of proteins, which in turn activates actin nucleation by the Arp2/3 complex (Figure 3)[30]. In addition to Rac, RhoA and Cdc42 are active in lamellipodial regions and contribute to lamellipodium extension[34]. RhoA might contribute to actin polymerization through a formin, while Cdc42 and integrins contribute to induce and maintain active Rac selectively at the leading edge of migrating cells. Negative feedback loops restrict the extent of Rac activation, including Arpin (inhibits Arp2/3 complex). RhoC acts further back in the cell, behind Rac, to downregulate cofilin activity and hence decreases actin polymerization, and stimulates actomyosin contractility (via Rho-associated protein kinase (ROCK)), which pulls the lamellipodial network rearwards. During migration, integrin based focal contacts need to be turned over, and this involves Rac itself, acting through PAK/GIT/β-PIX complex that is localized to focal contacts[30]. For melanoblasts and fibroblasts it is shown, that lamellipodia are not essential for migration. They can also migrate without Rac or the Arp2/3 complex, albeit more slowly. It is shown that cells compensate the absence of Rac or Arp2/3 by using filopodia or other protrusion in order to migrate[35].

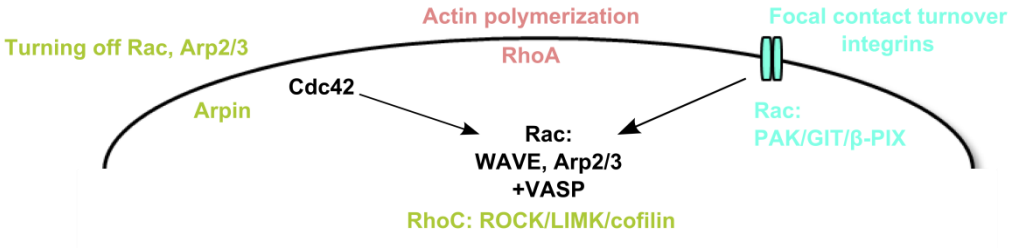

Figure 3 **Signalling in lamellipodia.** Rho family GTPases Cdc42, Rac1 and Rho act at different regions in a cell to orchestrate migration. Cdc42 generally controls the cell polarity and contributes to maintain Rac active at the leading edge. RhoA influences cell adhesion and maturation, in addition to controlling stress fiber formation and contractile activity. Rac primarily controls actin assembly and nascent adhesion formation in the lamellipodium (adapted from Ridley *et al.*[30]).

In contrast to lamellipodial migration, bleb-based migration is driven by cortical actomyosin contractility, and is associated with high levels of active RhoA/ROCK signalling[36]. The predominant Rho GTPase involved in bleb-driven migration is RhoA, acting through ROCK to stimulate myosin light chain phosphorylation (pMLC) and hence cortical actomyosin contractility. At the back of the cell, ezrin is associated with the actin cortex and reduces bleb formation. At the front of the cell, actomyosin contractility leads to focal detachment of the plasma membrane from the actin cortex to form blebs. Subsequently actin polymerizes on the bleb membrane to stabilize the protrusion, eventually leading to bleb retraction (Figure 4)[30].

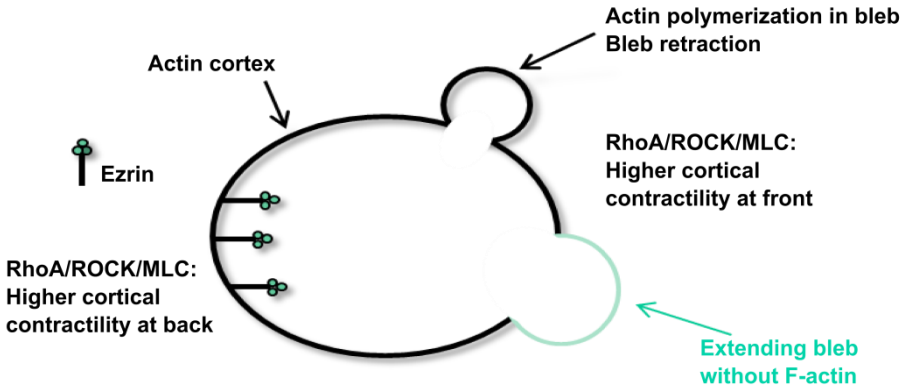

Figure 4 **Rho GTPases in bleb-driven migration.** Bleb-based migration is driven by cortical actomyosin contractility, and is associated with high levels of active RhoA/ROCK signalling (adapted from Ridley *et al.*[30]).

1.4 Artificial angiogenesis

Angiogenesis was first observed *in vitro* by Folkman and Haudenschild[37]. After long-term culture of capillary ECs, they observed the spontaneous organization of the cells into capillary-like structures. Additionally, they have confirmed the presence of a lumen by phase contrast microscopy and transmission electron micrography. This report of angiogenesis provided the basis for *in vitro* endothelial angiogenesis.

Depending on the way the cells reorganize, the commonly used assays can be roughly categorized into two categories: 2D (when ECs develop tubular structures on the surface of a substrate) and 3D (when ECs invade the surrounding matrix consisting of a biogel)[38,39].

1.5 Tube formation

In vivo, ECs are in contact on their basal surface with a thin, highly specialized ECM, the basement membrane. This matrix forms a sleeve around the ECs, and maintains the tube-like structures of the blood vessels[40,41]. Because EC tube formation on basement membranes replicates many steps in angiogenesis, it has been widely used as a screen for angiogenic and anti-angiogenic factors[42]. As a first screening assay it has many advantages. It is rapid, quantitative, and can be done in high throughput mode to screen large numbers of chemicals. Moreover it encompasses all steps in the angiogenic process: adhesion, migration, protease activity, alignment, and tube formation.

1.6 Hydrogels

Hydrogels are crosslinked polymer networks that absorb substantial amounts of aqueous solutions. They have attracted enormous research interest in the last years, because of the potential for a wide range of applications. Hydrogels have been successfully used in biomedical fields for example as wound dressings[43] and as cell-based therapeutics[44].

Hydrogels can be divided into two categories based on their natural or synthetic origins[45]. Hydrogel-forming synthetic polymers are prepared using chemical polymerization methods[46]. Natural polymers, which form hydrogels, include proteins such as collagen and gelatin, and polysaccharides such as alginate and agarose[47]. *In vitro*

growth matrices attempting to mimic the 3D environment of a cell, consist of a mixture of purified proteins such as collagen and laminin[48]. The most widely utilized example of an ECM extracted from living cells is the cell culture matrix commercialized as Matrigel[49,50]. Matrigel is an assortment of ECM proteins that have been extracted from Englebreth-Holm-Swarm tumors in mice[51] and is considered to be a reconstituted basement membrane preparation.

The complexity and dynamic structure of the endothelial basement membrane contributes to its various functions: Collagen IV contributes to the basement membrane's structural integrity and promotes cell adhesion and migration[40]. Heparan sulphate proteoglycans link collagen and laminin networks, bind soluble components, such as growth factors, and regulate the filtration activity of the basement membrane matrix[52]. The laminins are considered to be the major biologically active components of the basement membrane[53,54]. They organize and establish the basement membrane matrix and promote EC adhesion, migration and differentiation[55]. Thrombospondins inhibit EC proliferation and migration, by binding to many molecules in the basement membrane. Additionally, active antiangiogenic fragments have been identified[56]. Cells are tightly anchored to this matrix via cell surface receptors, including integrins, syndecans and dystroglycan.

Matrigel primarily consists of laminin, collagen IV and entactin and is mainly used to culture ECs, which start to build tubular structures when seeded on a Matrigel layer.

1.7 Aim of the study

Angiogenesis is the formation of new blood vessels out of pre-existing ones and is thus essential during development, but nonetheless, it also occurs in adults, during wound healing or diseases such as cancer[57].

The proliferation and migration of ECs is a central occurrence during the angiogenic process and although Blobel claimed that “3D trumps 2D when studying EC migration”[58], no detailed characterization of EC behavior in 3D exists up to now.

Thus the aim of this study was to characterize migration of HUVECs on Matrigel, which is commonly used as *in vitro* matrix for endothelial tube formation, as well as on a single cell basis, when cells are embedded in two structurally different hydrogels.

For this purpose, the main cues initiating endothelial tube formation should be elucidated, by analyzing biophysical (substrate rigidity and mechanotransduction), biochemical (secretion of growth factors, proteolysis) and cell biological (integrins) parameters. Furthermore, the experimental findings were implemented into simple mathematical models.

Concerning the analysis of single cells, the migration mode of ECs in 3D environments was analyzed. To investigate the impact of matrix composition on cell migration, the cells were embedded in structurally different hydrogels (spongy Matrigel and fibrillar rat tail collagen I gels), and cell morphology as well as migration parameters like contractility, polarization and adhesion were comparative studied and matched to the *in vivo* situation in the murine retina.

Concluding, this work aimed to elucidate the main regulator of endothelial tube formation on Matrigel and to characterize the migration behavior of ECs in hydrogels.

2 MATERIAL AND METHODS

2 MATERIAL AND METHODS

2.1 Material

All used equipment and consumables are listed in the Appendix 7.1. Pharmacological inhibitors are given in the Appendix 7.1.4. Primary and secondary antibodies for immunofluorescence are listed in Appendix 7.1.5. Fluorescent dyes (7.1.6) and hydrogels (7.1.7) are also listed in the Appendix. The composition of buffers is listed in the Appendix 7.1.8.

2.2 Methods

2.2.1 Cell culture

HUVECs

HUVECs were purchased from Promocell (Heidelberg, Germany) and maintained in endothelial cell growth medium (ECGM) containing 4.7% supplement mix, 10% fetal calf serum (FCS), 10.000 U/ml penicillin/streptomycin, 250 µg/ml amphotericin B under constant humidity at 37°C and with 5% CO_2. Experiments were performed using cells at passage #3.

Passaging

For passaging, medium was removed, cells were washed twice with phosphate buffered saline (PBS), trypsin/ethylenediaminetetraacetic acid was added and incubated at 37°C. After three minutes of incubation, digestion was stopped by adding stopping medium (10% FCS in M199). Cells were centrifuged (1000 rpm, 5 minutes, room temperature), resuspended in ECGM and, finally, transferred to a new flask or seeded for experiments.

Freezing and thawing

For long time storage, confluent HUVECs from a 75 cm^2 flask were trypsinized, centrifuged (1000 rpm, 5 minutes, room temperature) and resuspended in 3 ml ice-cold freezing medium (20% FCS, 10% dimethyl sulfoxide (DMSO) in M199). 1.5 ml aliquots were frozen in cryovials and stored at -80°C for 24 hours before being moved to liquid

nitrogen for longtime storage. In order to thaw cells, cryovials were warmed up to 37°C and the content was immediately dissolved in pre-warmed ECGM. DMSO was removed via centrifugation, cells were resuspended in ECGM and transferred to a 75 cm^2 flask.

Transfection of cells

For transfection of HUVECs the Targeffect-HUVEC kit was used. 250 000 cells/ml were seeded in a 6-well plate and incubated overnight. For transfection complex, 1000 µl DMEM were supplemented with 1 µg plasmid deoxyribonucleic acid (DNA), 5 µl targeffect and 15 µl peptide enhancer, with flicking the tube ten times after each addition. The mixture was incubated 25 minutes at 37°C and 5% CO_2. Afterwards, the medium of cells was removed and the transfection solution was added and incubated for two hours at 37°C, 5% CO_2.

2.2.2 Hydrogels

Rat tail collagen I gels

All solutions were placed on ice. In order to prepare collagen I gels with a final concentration of 1.0 mg/ml (1.5 mg/ml), 20 µl (20 µl) 10x endothelial basal medium (ECBM) were placed in a sterile tube. Then, 112 µl (79 µl) sterile H_2O, 8 µl (11 µl) $NaHCO_3$ 7.5%, and 50 µl (50 µl) 1x ECBM were added. After adding 60 µl (90 µl) of the collagen I solution (stock concentration 5 mg/ml), the content of the tube was mixed thoroughly. If desired, 18 x 10^6 HUVECs/ml were added to the mixture. For gelation, the gel was incubated at 37°C, 5% CO_2 for at least 30 minutes.

Matrigel

Matrigel was thawed on ice for several hours and mixed thoroughly for homogeneity after thawing and kept on ice. In order to reach final concentrations of 2.49 mg/ml and 4.15 mg/ml the gel was diluted with ice cold 1x ECBM. If desired, 18 x 10^6 HUVECs/ml were added. For gelation, the gel was kept at 37°C, 5% CO_2 for at least 30 minutes.

2.2.3 Retina preparation and imaging

Animals

Lifeact- enhanced green fluorescent protein (EGFP) transgenic mice have been previously described[59,60]. The expression of lifeact-EGFP is driven by a chicken actin promoter under the influence of a cytomegalovirus enhancer ensuring ubiquitous

expression[61]. Mice were kindly provided by Eloi Montanez, Walter Brendel Centre of Experimental Medicine and Munich Heart Alliance, Ludwig-Maximilians-Universität, Munich, Germany. All experiments with mice were performed in accordance to the German guidelines and regulations. The protocols were approved by the Committee on the Ethics of Animal Experiments of the Ludwig-Maximilians-Universität, Munich, Germany.

Preparation and imaging of fixed postnatal day three (P3) mouse retina

The retina was explanted from P3 mice eyes as previously published[62]. The eye was fixed in 4% para-formaldehyde (PFA) at room temperature for two hours. The vitreous body and the lens were removed, the retina was extracted and cut into four equal quadrants from the rim to half of its radial length. The retina was blocked and permeabilized by retina blocking buffer over night at 4°C. The blocked retina was washed with PBlec three times for 20 minutes, each. After washing, the retina was incubated with isolectin GS-B_4, Alexa 488 conjugate 1:25 and primary antibodies 1:100 in retina blocking buffer overnight at 4°C. The retina was washed with retina wash buffer (retina blocking buffer/PBS, 1:1) five times for 20 minutes, each. Secondary antibodies were diluted 1:400 in retina blocking buffer and incubated two hours at room temperature, followed by washing with retina wash buffer (4x 20 minutes). Prior to microscopy a drop of mounting medium FluorSave™ Reagent was placed on the retina and the retina was covered by a glass coverslip.

Preparation and live-imaging of P3 mouse retina

The retina was explanted from P3 mice eyes without fixation of the eye and cut into four equal quadrants from the rim to half of its radial length as described in the section before. To take the retina into *in-situ* culture, the retina was placed in one well of µ-Slide 8 Well and fixed at the bottom of the well with 10 µl Matrigel. The retina was covered with a glass coverslip afterwards. After 60 minutes incubation at 37°C, 5% CO_2 the retina was covered with 200 µl DMEM, 10% FCS, 1.25 µg/ml amphotericin B. Confocal imaging of live vessel growth was performed using a laser-scanning confocal microscope with Plan Apochromat 63x/1.3 NA glycerol objective using LAS X Core Software (Leica, Wetzlar, Germany). 3D image projection and volume rendering was performed using IMARIS ([IMARIS x64 7.6.5] Bitplane, Zurich, Switzerland). The surface area detail level was set to 0.4 µm for images and 0.6 µm for movies. After the image rendering a volume and intensity threshold was set. Live imaging was performed at 37°C, 5% CO_2 and 80% humidity.

2.2.4 Rheology of hydrogels

The quantification of the elastic modulus of the hydrogels was performed on a stress-controlled macrorheometer with a 25 mm plate-plate geometry at a plate separation of 200 µm using a torque of 0.5 µNm and a frequency of 1 Hz ensuring linear response. The rheometer plate was cooled to 5°C before 150 µl of the samples were added, and gelation was induced by a sudden temperature change to 37°C. An applied oscillatory stress $\sigma = \sigma_0 \sin(\omega t)$ with a frequency ω resulted in an oscillatory strain with the same frequency, $\gamma = \gamma_0 \sin(\omega t + \delta)$, where δ denotes the phase shift between stress σ and strain γ. With those parameters, the storage modulus $G' = \sigma_0 / \gamma_0 \cos(\delta)$ can be calculated, which is a measure for the elastic property of the gel.

2.2.5 Immunostainings

Immunostaining of hydrogels

6 µl of the desired gel were filled into the observation channel of µ-Slide Chemotaxis^{3D}. Staining-solutions were filled into the reservoirs. The polymerized gel was fixed with 2% glutaraldehyde in PBS for 40 minutes and washed afterwards with PBS for 30 minutes. The gels were blocked with 1% bovine serum albumin (BSA) in PBS overnight. Primary antibodies were diluted 1:100 in 1% BSA and gels were incubated for 72 hours. Before incubation of secondary antibodies (1:200 in 1% BSA), the gels were washed twice with PBS for 30 minutes. The incubation of secondary antibodies was for 48 hours. Prior to microscopy, the gels were washed again with PBS for 30 minutes. Afterwards, the PBS was renewed and kept in the reservoirs during confocal microscopy.

Immunostaining of HUVECs

HUVECs embedded into hydrogels were fixed with 4% PFA for 40 minutes and washed with PBS twice for 20 minutes. The cells were permeabilized for 20 minutes with 0.5% Triton X-100 in PBS and washed afterwards with PBS for 30 minutes. The cells were blocked with 1% BSA in PBS overnight. Primary antibodies were diluted 1:100 with 1% BSA in PBS and cells were incubated for 72 hours. Prior to incubation with secondary antibodies (1:200 in 1% BSA) the cells were washed twice with PBS for 30 minutes. The cells were incubated with secondary antibodies for 48 hours. Afterwards the cells were washed with PBS for 30 minutes and stained with rhodamine phalloidin (1:400 in 1% BSA) and Hoechst 33342 (0.5 µg/ml) for 40 minutes. Prior to microscopy the cells were washed again with PBS for 30 minutes. Finally, the PBS was renewed and kept in the reservoirs during confocal microscopy.

Confocal microscopy of hydrogels and HUVECs

Confocal images were collected using a laser-scanning confocal microscope with Plan Apochromat 63x/1.4 NA oil, 63x/1.3 NA glycerol, 63x/1.2 NA water objectives using LAS X Core Software (Leica, Wetzlar, Germany). All imaging was performed at room temperature.

2.2.6 Single cell migration

3D chemotaxis

3D chemotaxis experiments were conducted according to the manufacturer's instructions (ibidi, Martinsried, Germany). After reaching confluency, HUVECs were trypsinized and embedded into rat tail collagen I gels or Matrigel as described in chapter 2.2.2. Finally, the gels were filled into the µ-Slide Chemotaxis^{3D}. 1x ECBM was used as attractant-free medium, while ECGM supplemented with 10% FCS was used as chemoattractans, in order to analyze the chemotactic effect on migration of HUVECs.

Phase contrast and fluorescent microscopy for live cell imaging

Time-lapse video microscopy with HUVECs was performed using an inverted microscope Eclipse Ti, a 4x phase contrast objective, and a charge coupled device (CCD) camera with a time interval of ten minutes between images. The slides were inserted into a 37°C heating and incubation system. The system was flushed with actively mixed 5% CO_2 at a rate of ten l/hour. The humidity was kept at 80% to prevent dehydration.

Cell tracking and image analysis

Time-lapse video microscopy was performed over a time period of 21 hours. The time-lapse interval was ten minutes. Cell tracking was performed using the ImageJ software (National Institutes of Health, Bethesda, USA) plugin "Manual tracking" (Fabrice Cordelières, Institut Curie, Orsay, France). Each experiment was repeated three times, completely independent from each other. On average 20-30 cells were tracked per experiment. To further analyze and evaluate chemotactical processes and cell migration velocities, the "Chemotaxis and Migration Tool" (ibidi, Martinsried, Germany) was used. For quantification of chemotaxis and migration, the forward migration indices (FMIs) in parallel and perpendicular to the direction of the gradient, the cell velocity and the directness of cells were evaluated[63].

Accumulated distance

The accumulated distance $d_{i,accum}$ for each cell was calculated as the sum of all incremental movements measured in between all m single images. The average accumulated distance d_{accum} is the average over all $d_{i,accum}$, where m is the number of all analyzed images and $d_{i,j}$ is the displacement of the cell number i from image j-1 to image j.

$$d_{accum} = \frac{1}{n} \sum_{i=1}^{n} d_{i,accum};\ d_{i,accum} = \sum_{j=2}^{m} d_{i,j}$$

Forward migration indices parallel and perpendicular to the gradient

The $FMI_{\parallel}$, $FMI_{\perp}$ represent the efficiency of forward migration of cells parallel and perpendicular to the gradient, respectively. For experiments shown in this thesis we chose the coordinate system such that the y-axis was parallel to the gradient and the x-axis was perpendicular to the direction of the gradient.

$$FMI_{\parallel} = \frac{1}{n} \sum_{i=1}^{n} \frac{y_{i,end}}{d_{i,accum}};\ FMI_{\perp} = \frac{1}{n} \sum_{i=1}^{n} \frac{x_{i,end}}{d_{i,accum}}$$

Euclidian distance

The Euclidian distance $d_{i,euclid}$ for each cell was calculated as the length of the straight line between the cell start and end point. The average Euclidian distance d_{euclid} was calculated as the average over all $d_{i,euclid}$.

$$d_{euclid} = \frac{1}{n} \sum_{i=1}^{n} d_{i,euclid};\ d_{i,euclid} = \sqrt{(x_{i,end} - x_{i,start})^2 + (y_{i,end} - y_{i,start})^2}$$

Directness

The directness (D) represents a cell's tendency to travel in a straight line. It was calculated by dividing the Euclidian distance by the accumulated distance for each cell. D_i is the directness of one single cell, D is the average of all values of directness for all cells.

$$D = \frac{1}{n} \sum_{i=1}^{n} D_i = \frac{1}{n} \sum_{i=1}^{n} \frac{d_{i,euclid}}{d_{i,accum}};\ D_i = \frac{d_{i,euclid}}{d_{i,accum}}$$

2.2.7 Tube formation assay

HUVEC tube formation assay was performed in µ-Slide angiogenesis. Matrigel was thawed on ice for several hours, mixed thoroughly for homogeneity and kept on ice. Pipette tips as well as the µ-Slide angiogenesis were kept on ice for the whole experiment. The inner well of the slide was filled with 10 µl Matrigel. For gelation, the gel was kept at 37°C, 5% CO_2 for at least 30 minutes. After reaching confluency, HUVECs were trypsinized and diluted to the desired concentration. 50 µl of the desired concentration of cells was applied to the upper well of the slide. The slide was covered by the supplied lid

and incubated at 37°C and 5% CO_2. Either live imaging was performed or images were taken after a desired period of time.

2.2.8 Polyacrylamide gels coated with Matrigel

Cleaning and activation of glass coverslips

Glass coverslips were cleaned in an ultraviolet (UV) cleaner for 15 minutes. Afterwards the coverslips were carefully placed in a stainless steel rack, which was filled with 99.8% ethanol. The rack was placed in an ultrasound bath for five minutes. The ethanol was discarded afterwards and the rack was refilled with 2% (3-aminopropyl) trimethoxysilane (APTES) in ethanol (99.8%) and incubated for 15 minutes in ultrasound. The coverslips were washed by immersing the rack in two changes of ethanol (95%). Afterwards the rack was removed from ethanol and dried in an oven (~30 minutes, 70°C). While cooling the rack, 0.5% glutaraldehyde solution in ddH_2O was prepared. The round coverslips were immersed in the glutaraldehyde solution for 30 minutes at room temperature. The coverslips were washed in ultrasound with ddH_2O for 15 minutes. A small amount of dichlordimethylsilane (DDS) was placed on the square coverslips, to increase hydrophobicity, until the coverslip was completely covered by a thin layer of DDS and incubated for 10 minutes. Afterwards the DDS was wiped off from the coverslips and they were rinsed with ddH_2O.

Preparation of the polyacrylamide substrate

Acrylamide, bis-acrylamide, and PBS were mixed to produce the desired gel stiffness in a 15 ml conical tube. An appropriate amount of acrylamide solution was placed into a 1 ml tube, 1:100 volume of ammonium persulfate (APS) and 1:1000 volume of tetramethylethylenediamine (TEMED) were added to the gel solution. After mixing, 35 µl of the gel mixture were quickly pipetted onto the aminosilanated coverslips, before the chlorosilanated coverslips were placed on top of the polymerizing gel solution. The gels polymerized on wet paper towels under a petri dish for 60 minutes. After polymerization was completed the surface of the slides was flooded and the gels were covered with 50 mM HEPES. The chlorosilanated coverslips were removed and the gels were placed into fresh 50 mM HEPES.

Cross-linking ECM to the polyacrylamide sheet

Excess HEPES was wicked off with a lint-free tissue before the coverslip was placed in a 6-well plate under a UV-light. 200 µl of sulfo-SANPAH cross-linker (0.4 mM in ddH_2O) were added to the polyacrylamide (PAA) surface. For using short-wavelength (300-

350 nm) UV-light lamps, the gel had to be placed in a distance of 8 cm to the lamp. After 10 minutes of UV treatment, the coverslip was washed in PBS to remove excess sulfo-SANPAH. The UV-light activation step was repeated two times.

Matrigel coating and seeding of HUVECs

Matrigel was thawed on ice for several hours, mixed thoroughly for homogeneity, and kept on ice. The spin coater was located in a cold room (~4°C). The coverslip coated with the PAA gel was placed on the rotation table of the spin coater, with the PAA gel on top. After reaching maximum speed (10 rps) 150 µl Matrigel were pipetted on the PAA gel. The rotation after adding Matrigel lasted 20 seconds. Afterwards, the coverslip was placed in a 6-well plate and fixed on the bottom of the plate with solvent-free nail polish. The Matrigel was allowed to polymerize for 30 minutes at 37°C and 5% CO_2. A desired concentration of HUVECs in ECGM was seeded on the gel and investigated for tube formation.

2.2.9 Traction force microscopy

Glass coverslips (8x8x0.17 mm) and µ-Slide 8-well (uncoated) were cleaned in an UV cleaner for 2x 15 minutes. Afterwards the hydrophobicity of the coverslips was increased by DDS (10 minutes), they were washed with ddH_2O and finally dried off. The 8-well slides were treated with 0.5% glutaraldehyde solution in ddH_20 for 30 min, and afterwards washed two times with ddH_2O. Yellow-green microbeads of 1 µm diameter, 2% solids were mixed with Matrigel (1:750). 30 µl of the bead/Matrigel mixture were pipetted into the 8-well slide. The gel was gently pressed on by a coverslip and incubated for 30 minutes at 37°C, 5% CO_2, before 250 000 cells/ml were seeded on the gel. Fluorescent microscopy was performed according to chapter 2.2.6. Data were analyzed by Andriy Goychuk, Arnold Sommerfeld Centre for Theoretical Physics and Centre for NanoScience, LMU Munich.

2.2.10 Microfluidics

For cultures under flow conditions the channels (µ-Slide I Luer) were coated with Matrigel (100 µl per slide) and kept at 37°C, 5% CO_2 for at least 30 minutes. HUVECs (5 x 10^5 per cm^2) were seeded into the channels with a micropipette, and the cells could attach to the gel within 20 minutes under static conditions at 37°C, 5% CO_2. Afterwards the channel slide was inserted into a 37°C heating and incubation system. The system was flushed with actively mixed 5% CO_2 at a rate of ten l/hour and placed on an inverted microscope

Eclipse Ti. The humidity was kept at 80% to prevent dehydration. Fresh medium was then pulled through the channel at a flow rate of 0.1 ml/minute for six hours.

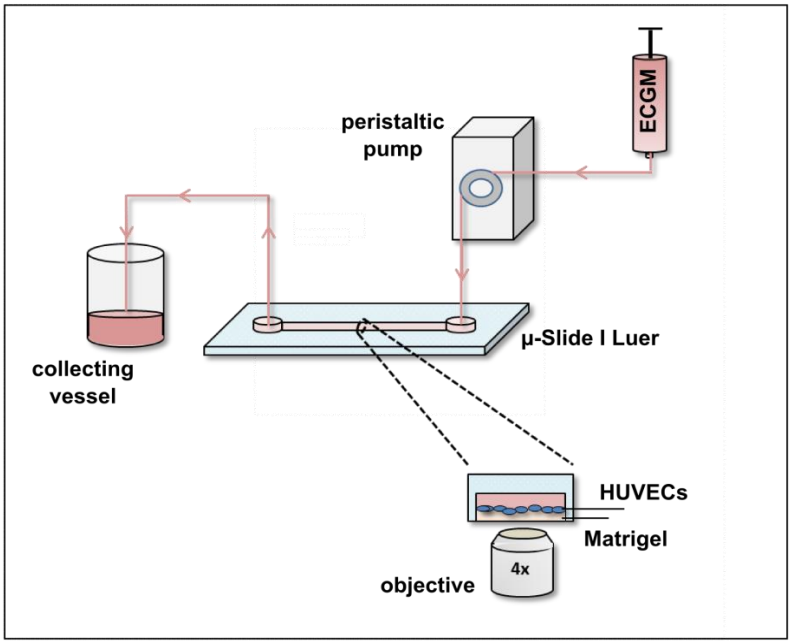

Figure 5 **Illustration of the microfluidic experiment**. HUVECs were seeded in Matrigel-coated µ-Slide I Luer. Cells were cultured at a constant flow rate of 0.1 ml/minute for six hours.

2.2.11 Statistical evaluation

The data are presented as the mean value from three independent experiments with the corresponding SD or SEM. Statistical tests were student's *t*-test performed using Excel (Microsoft Corp., Redmond, WA) or Prism software (GraphPad Software). The differences were statistically significant at P≤0.001 (indicated on graphs as triple asterisks), P≤0.01 (indicated as double asterisks), or P≤0.05 (indicated as single asterisk).

3 RESULTS

3 RESULTS

3.1 Spatio-temporal characterization of endothelial tube formation

3.1.1 Formation of cell-cell contacts depends on the mean distance between single cells

To investigate the impact of the cell number on network formation of ECs, we prepared tube formation assays on Matrigel with different cell densities. At a low density of HUVECs (60 000 cells/ml) plated on Matrigel, the cells barely moved and no network formation took place (Figure 6A). Rather than forming cords, the cells simply stayed separate. At 100 000 cells/ml, the cells could stretch and gain cell-cell contacts. Initial network connections were made, and cords were formed. At higher densities such as 140 000 cells/ml, 200 000 cells/ml and 280 000 cells/ml, cells formed a more defined and compact network. At 340 000 cells/ml, the cells condensed into large islands of cells and did not form tubular structures, the network connections were built out of cell clusters. These observations were confirmed in the quantitative analysis of the images, shown in Figure 6B. The number of tubes increased up to 280 000 cells/ml, while it was reduced at 340 000 cells/ml. The other parameters were consistently increasing with higher cell numbers. Viewed together, Figure 6 shows that a minimum cell density of 100 000 cells/ml is required for network formation and increased cell density leads to an increased network formation.

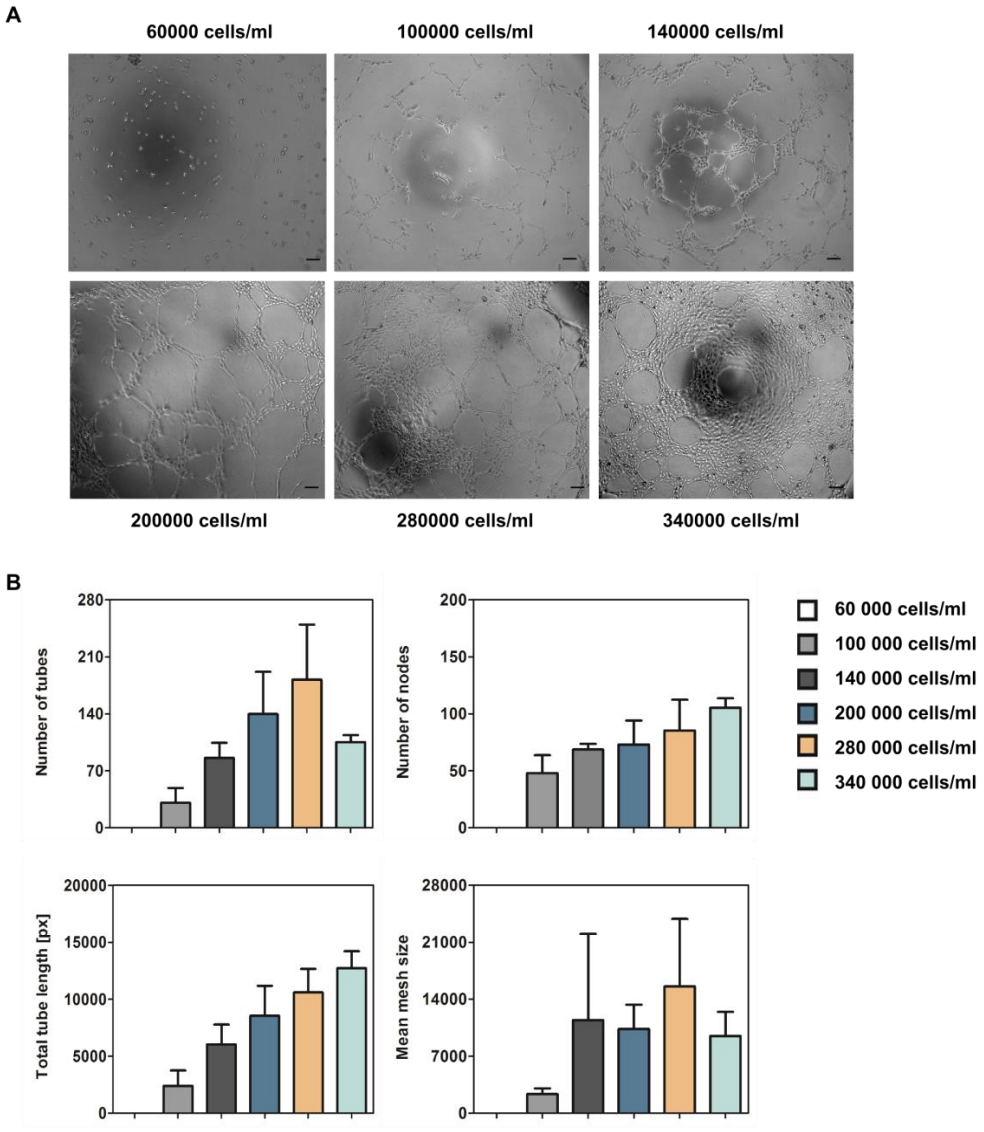

Figure 6 **A minimum cell density is required for network assembly.** HUVECs were seeded on Matrigel with different cell densities. (**A**) At least 100 000 cells/ml were necessary to induce tube formation, while in lower cell numbers, HUVECs stayed separate and were too sparse to form a network. Images were taken after six hours. (**B**) Quantification of number of tubes, nodes, total tube length and mean mesh size showed an increase in all parameters with increasing cell densities. If the cell density is too high (340 000 cells/ml), cell clusters were formed, followed by a decreased number of tubes (n=3). Bars, 100 µm.

The dependence of the cell movement direction on the position of the nearest neighbouring cell is shown in Figure 7. The angle (C_{nn}) between the direction of movement of a cell and the direction in which the nearest neighbour of the cell is located is shown exemplarily for 200 000 cells/ml (Figure 7A). This graph indicates that the movement directions of the nearest neighbouring cells are highly correlated thus, nearest neighbours move in the same direction almost all the time, before they build clusters and consequently stick together and move in the same direction. The time required for nearest

neighbouring cells to find each other (τ) decreased with increasing cell densities (Figure 7B). This showed that the higher the cell densities, the faster the cells find each other, with the exception of 340 000 cells/ml. This might be due to image analysis, where it is difficult to analyse single cells at such a high cell density.

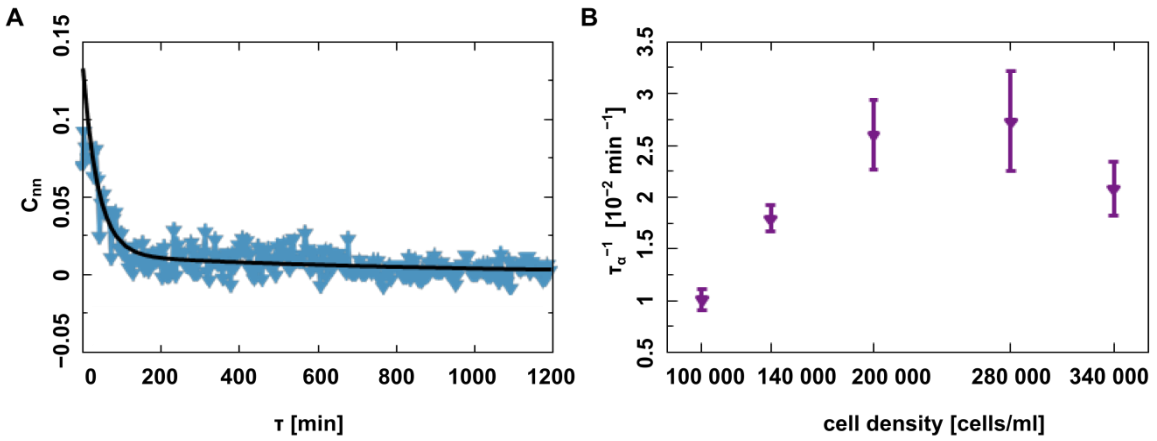

Figure 7 **Relative motion of the cell population is a directed process.** (A) The angle (C_{nn}) between the movement direction of a cell and the direction in which its nearest neighbouring cell is located, with a cell density of 200 000 cells/ml. (B) Biexponential fit, with the inverse exponent τ_α^{-1} against the cell density. The inverse exponent showed that with increasing cell densities, the cells took less time to find its nearest neighbour (n=3). *In collaboration with Andriy Goychuk, Arnold Sommerfeld Centre for Theoretical Physics and Centre for NanoScience, Department of physics, LMU Munich*.

3.1.2 Morphogenesis is not based on soluble or matrix bound gradients of growth factors

It has been shown that ECs migrate chemotactically in gradients of VEGF[64]. It is unknown, however, if the existence of a VEGF gradient initiates the formation of cells and thus, starts the process of tube formation. As shown in immunostainings and intensity profiles in Figure 8A, there was no matrix bound gradient of VEGF (green) between single cells, or tubular structures, respectively. At the starting point (0 hours), the fluorescence intensity of VEGF (green) was evenly distributed with small intensity peaks at the cells, but without a gradient. The intensity plot after three hours showed an equal progression: The intensity of VEGF bound to the matrix, was at a basal level, while there were intensity peaks at the areas covered by cells, respectively tubes. A matrix-bound gradient of VEGF between single cells or tubes was not detectable at early steps of tube formation. Having shown that matrix bound gradients of VEGF do not exist and thus cannot direct cell movement, we further investigated the impact of soluble VEGF gradients. We saturated the VEGF concentration by adding 20 nM to the EC growth medium (Figure 8B). As controls we

analyzed endothelial tube formation for HUVECs seeded in growth medium as well as in PBS containing calcium and magnesium. After three and six hours we detected no hindrance of endothelial tube formation by saturating VEGF gradients. Even more, we could show that endothelial tube formation is independent of external growth factors, too, since the formation of tubes and nodes is not inhibited, when cells were seeded in PBS+Ca^{2+}, Mg^{2+}. To specifically avoid the formation of soluble gradients in the medium, we performed microfluidic experiments, where HUVECs were cultured on Matrigel at a constant volume flow of 0.1 ml/minute (Figure 8C). This showed that the initial pattern formation of cells, as well as the formation of tubular structures was not hindered by a constant flow of EC growth medium, which avoids the formation of a soluble gradient. Recapitulatory, the formation of tubular structures in the EC tube formation assay on Matrigel does not depend on matrix bound or soluble gradients of VEGF.

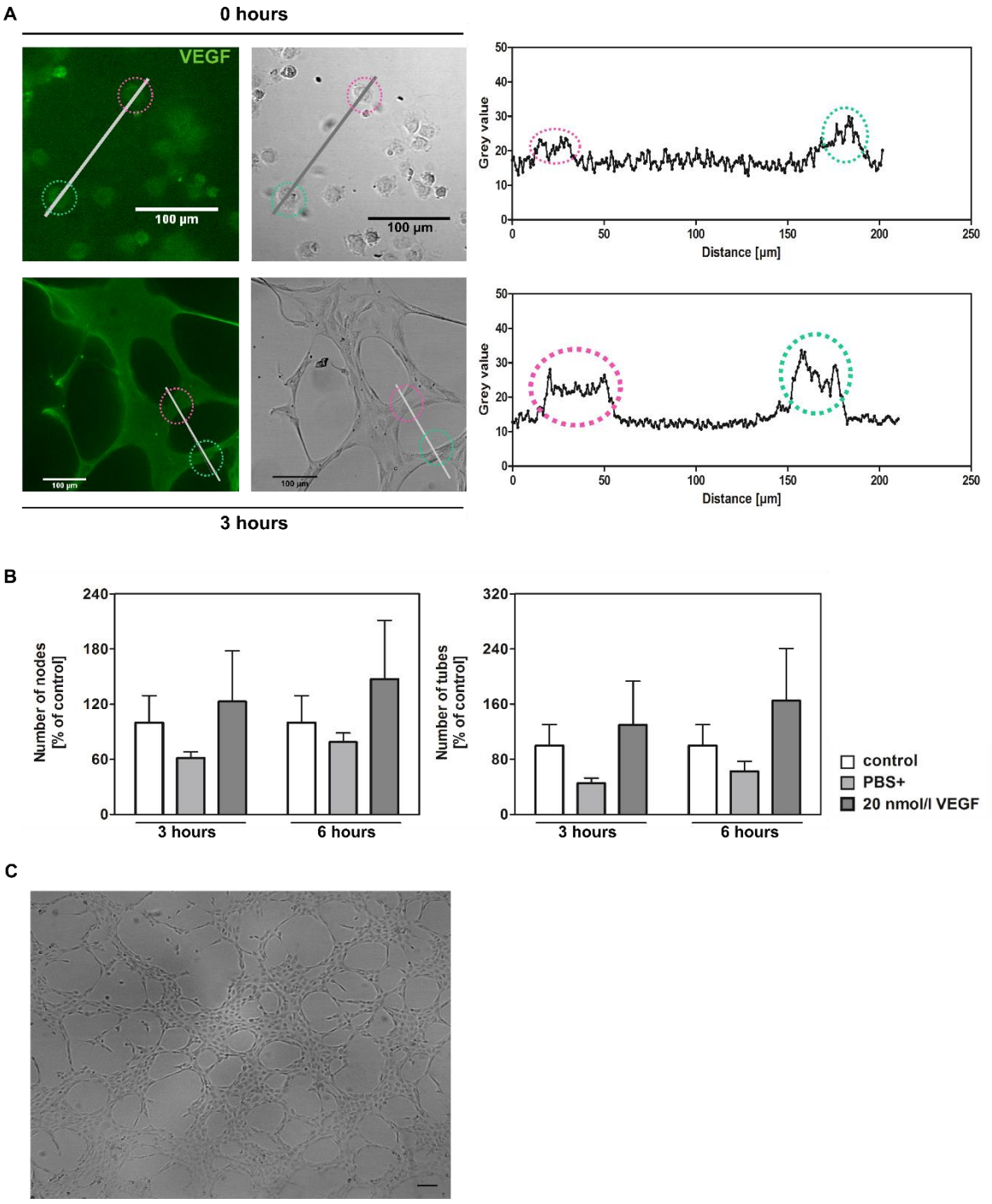

Figure 8 **Neither bound nor soluble gradients are critical for EC tube formation.** (**A**) HUVECs were seeded on Matrigel at 200 000 cells/ml in ECGM and fixed with 4% PFA 0, and 3 hours after adhesion to the matrix. Immunostaining of VEGF and subsequent analysis of intensity profiles showed no bound VEGF gradient over time. Intensity profiles were analyzed using ImageJ software. (B) Quantification of number of nodes and tubes after saturation of soluble VEGF gradients by 20 nM VEGF had no impact on the formation of tubular structures. HUVECs (200 000 cells/ml) were analyzed 3 and 6 hours after seeding on Matrigel. Control cells were seeded in ECGM (control) and PBS containing Ca^{2+} and Mg^{2+} (PBS+). (**C**) Microfluidic experiments of HUVECs seeded into µ-Slide I Luer, coated with Matrigel. The channel was flushed with ECGM at 0.1 ml/minute and image was kept after six hours. The absence of soluble gradients did not impair HUVEC tube formation (n=3; *P≤0.05). Bars, 100 µm.

3.1.3 Cells actively deform their substrate to attract other cells

To analyse whether ECs communicate via cellular forces exerted on the matrix, we investigated the deformation of the matrix by cells. We embedded fluorescent microbeads into Matrigel and seeded HUVECs (200 000 cells/ml) on the gel (Figure 9). The analysis of the bead displacement over the first 50 minutes after seeding the cells on Matrigel, revealed a clear force exerted on the underlying matrix, as seen by bead movement towards cells (Figure 9A, left image). Investigating an exemplary single cell (white asterisk), we could show that this cell is attracted by the forces exerted by the cell, focused with the blue asterisk (Figure 9A). Furthermore, we could show that the velocity of bead movement, representing cellular forces exerted on the matrix, decreases over time (Figure 9B). That implies that cells first deform the matrix, and afterwards form the network. By colour coding of bead density we could show that beads were evenly distributed and do not form aggregates, which might otherwise distort the displacement of single beads.

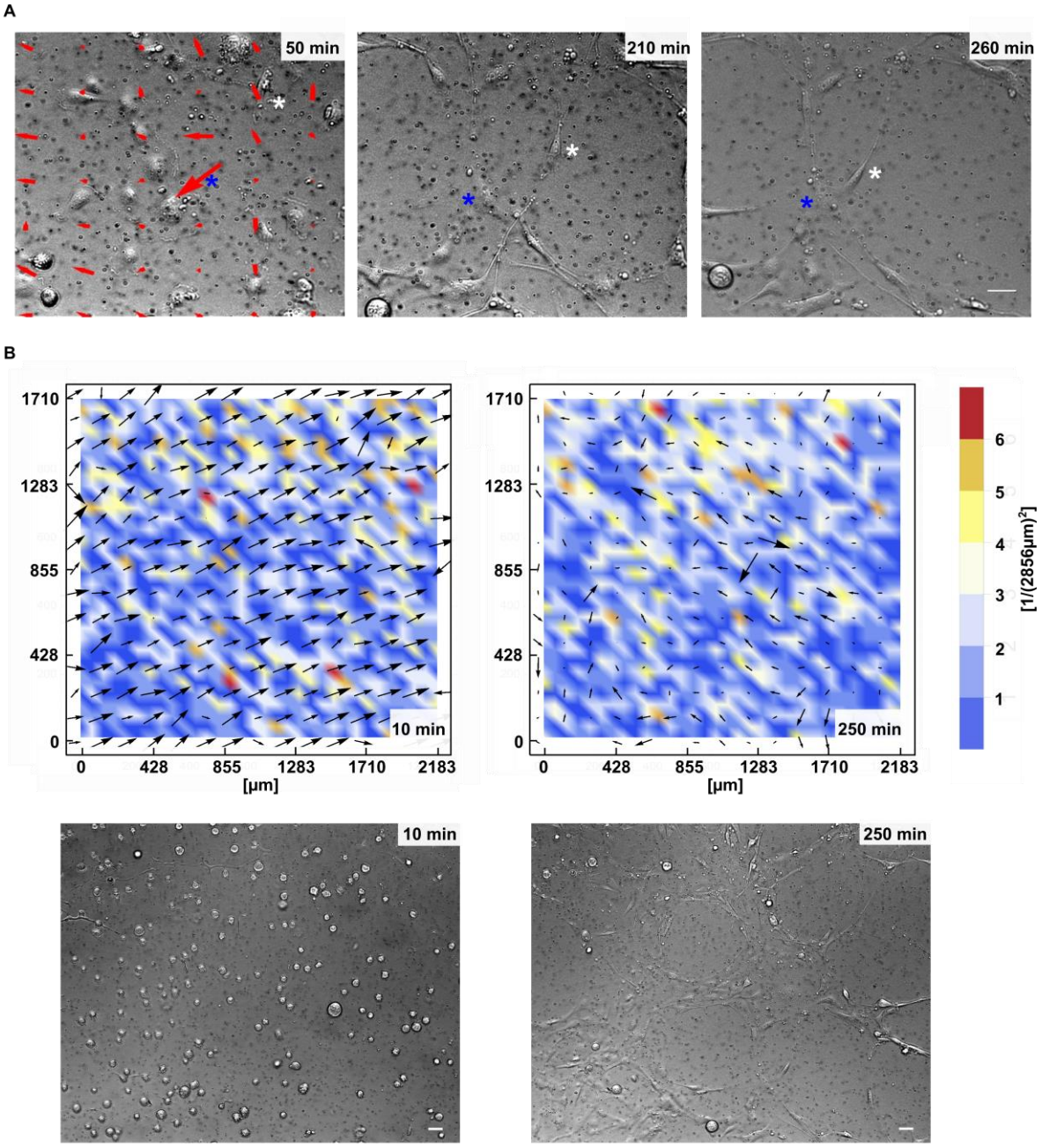

Figure 9 **HUVECs exert forces on the ECM.** HUVECs (200 000 cells/ml) were seeded on Matrigel, containing fluorescent beads. (**A**) Left image: Analysis of bead velocity over 50 minutes. The red vectors represent the velocity of bead movement, indicating applied force. The direction of the vectors indicates the averaged direction of bead movement. Blue asterisk focuses an exemplarily cell exerting high mechanical forces on the matrix, at three different time points (50, 210 and 250 minutes). The white asterisk focuses a cell, which migrates in the direction of these forces. (**B**) The direction of vectors indicates the averaged direction of bead movement at two different time points (10 and 250 minutes). Colour codes show local density of beads. The velocity of bead movement is represented by the length of each vector, indicating that the applied forces decrease over time. Images in the lower panel show cells at respective time. Bars, 100 µm. *(Vectors were analyzed by Andriy Goychuk)*.

3.1.4 Endothelial tube formation with different cell-to-cell distances depends on the rigidity of the matrix

Besides the matrix composition, the substrate rigidity might influence the adhesion and migration of cells. We created PAA gels with defined stiffness and coated them with Matrigel (Figure 10A). To this end we coated coverslips with PAA gels with controlled stiffness between 3 and 5000 Pa and seeded different numbers of HUVECs on the gels. Figure 10A shows that different cell densities are needed for a respective substrate rigidity, in order to allow for optimum EC tube formation. In Figure 10B the cell densities are plotted against the respective gel rigidity, which allows for optimum tube formation. The graph indicates that for lower cell densities higher substrate stiffness is necessary to promote tube formation, while for higher cell numbers soft gels provide the best substrate for the building of tubules.

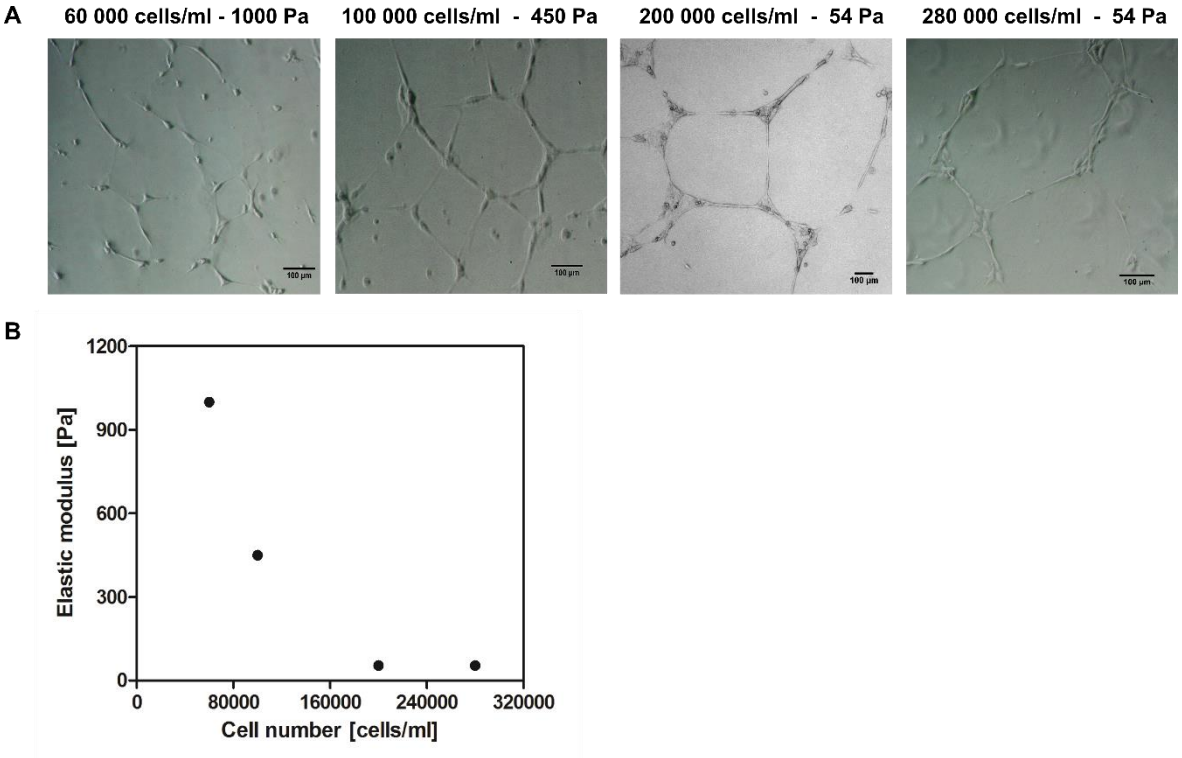

Figure 10 **Matrix stiffness influences endothelial tube formation.** (**A**) HUVECs were seeded on PAA gels with different stiffness, coated with Matrigel, at 60 000, 100 000, 200 000 and 280 000 cells/ml. Images were taken after nine hours. The gel stiffness optimally promoting tube formation is shown for each cell density. (**B**) Cell number plotted against the elastic modulus, which is ideal for tube formation at the respective cell density. Bars, 100 µm.

3.1.5 Proteolytic activity is not essential for the formation of tubes

Extracellular proteolysis has been implicated in many steps of the angiogenic processes, including basement membrane degradation, cell migration, and capillary lumen formation[65]. To investigate the role of matrix metalloproteinases (MMPs) for endothelial tube formation on Matrigel, we inhibited a broad range of MMPs with 10 µM batimastat (Figure 11). Visually (Figure 11A) as well as quantitatively (Figure 11B), we could not detect any hindrance of the tube formation process after batimastat treatment of cells. On the contrary, the formation of tubular structures is enhanced by batimastat treatment.

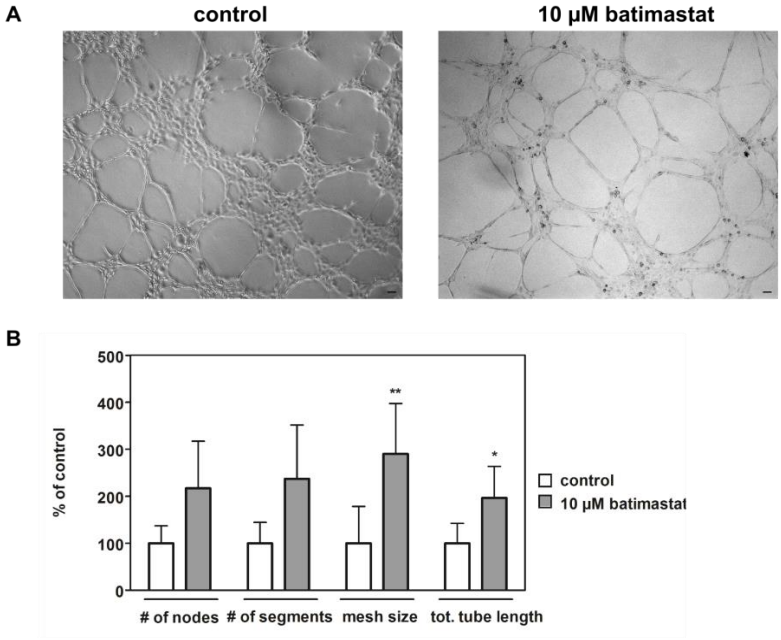

Figure 11 **HUVEC tube formation is not hindered by inhibition of MMPs**. (**A**) HUVECs were seeded on Matrigel at 200 000 cells/ml in ECGM as control and with 10 µM batimastat to inhibit MMP activity. Images were taken after six hours. (**B**) Quantitative analysis of the number of nodes and segments, mesh size and total tube length showed that the activity of MMPs is not crucial for HUVEC tube formation (n=3; *P≤0.05; **P≤0.01). Bars, 100 µm.

3.1.6 Cell adhesion to laminin is essential for endothelial tube formation

In the context of mechanotransduction we investigated the importance of the interaction between integrins and ECM proteins for EC tube formation. Therefore we used different integrin-blocking antibodies (Figure 12). While inhibition of integrin binding to fibronectin and other ECM proteins (integrins α_4, α_5 and α_v) did not influence endothelial tube formation, blocking of integrin binding to laminin (integrins α_1, α_2, α_3 and α_6) potently

inhibits the formation of nodes and tubes. This indicates that laminin is a crucial matrix component for the formation of tubes.

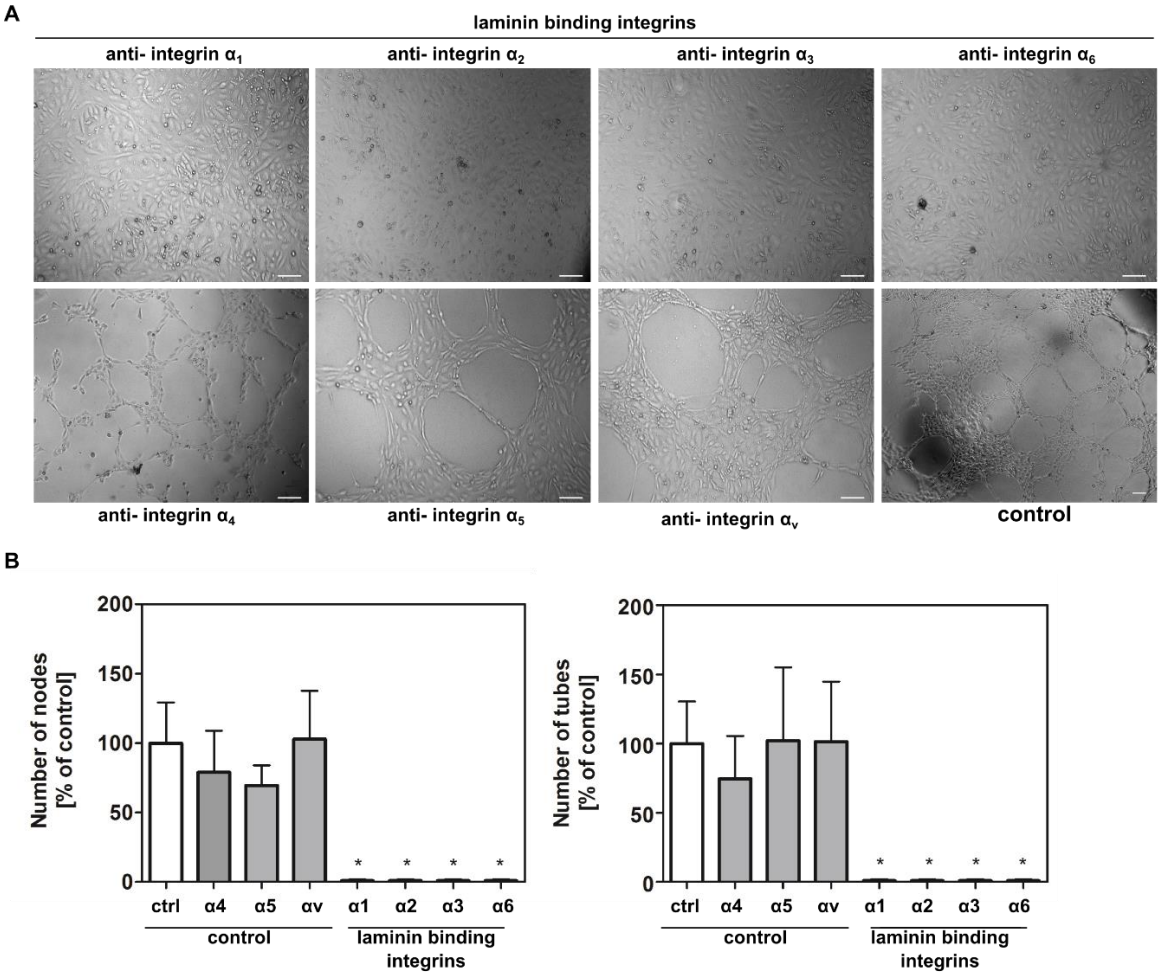

Figure 12 **Adhesion to laminin is crucial for endothelial tube formation.** (**A**) HUVECs were seeded on Matrigel at 200 000 cells/ml in ECGM. To investigate the role of adhesion to different matrix proteins, antibodies against integrins α_1, α_2, α_3, α_4, α_5, α_6 and α_v were added (40 µg/ml). Images were taken after six hours. (**B**) Quantitative analysis of the number of nodes and tubes, showed that blocking of laminin binding integrins (α_1, α_2, α_3 and α_6) significantly decreased the number of nodes and tubes, while blocking of collagen and fibronectin binding (integrins α_4, α_5 and α_v) did not affect endothelial tube formation (n=3; *P≤0.05). Bars, 100 µm.

3.1.7 Contractility impacts endothelial tube formation

It has been shown that contractility plays a pivotal role in mechanotransduction[12]. Therefore we investigated the role of cellular contractility for endothelial tube formation, by treatment of cells with the myosin II ATPase inhibitor blebbistatin (10 µM) (Figure 13). Due to myosin II inhibition initial pattern formation was hindered and tubular structures were not detectable (Figure 13A). The quantitative analysis confirmed this observation by a

significantly reduced number of nodes and a reduction in the number of tubes (Figure 13B).

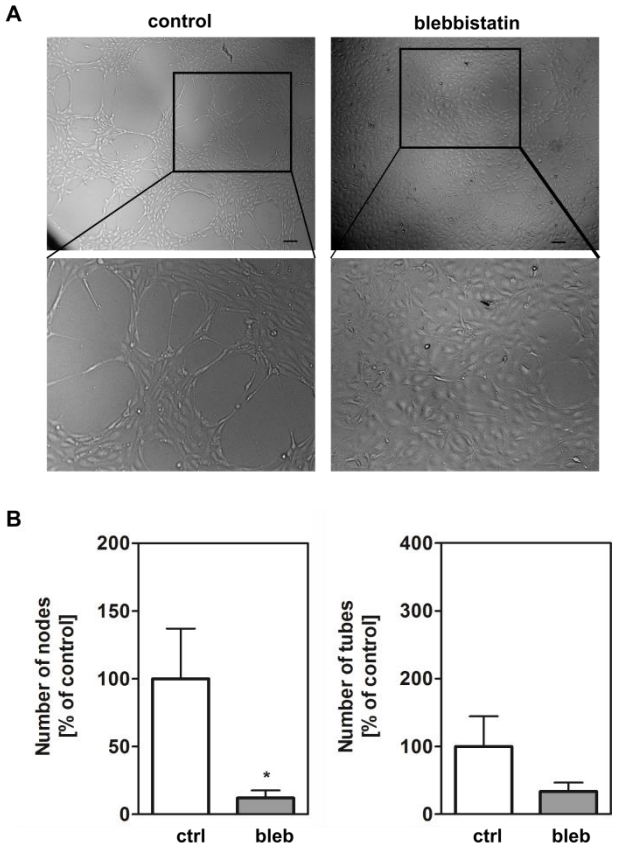

Figure 13 **Inhibition of contractility hinders endothelial tube formation.** (**A**) HUVECs were seeded on Matrigel at 200 000 cells/ml in ECGM as control, and treated with 10 µM blebbistatin to inhibit contractility of cells. Inhibition of contractility using blebbistatin hindered the formation of tubular structures. (**B**) Images were taken after six hours and analyzed on the number of nodes and tubes (n=3; P≤0.05). Bars, 100 µm.

3.1.8 Simulation of endothelial tube formation shows a directed, force dependent process

The above stated experimental results were taken as assumptions to adapt a numerical model of endothelial tube formation. Using an extension of the Cellular Potts Model on a triangular lattice, random, chemotactic and directed cell migration were compared (Figure 14). Here, we could show that simulations for random, as well as chemotactic migration (Figure 14A and B) did not result in the formation of tubular structures after 1000 Monte Carlo steps (MCS). In contrast, confirming the experimental results, a directed migration process based on mechanotransduction (Figure 14C) showed the formation of a compact network after 1000 MCS. The simulations were performed by

Andriy Goychuk as part of his master's thesis at the Arnold Sommerfeld Centre for Theoretical Physics and Centre for NanoScience (LMU Munich).

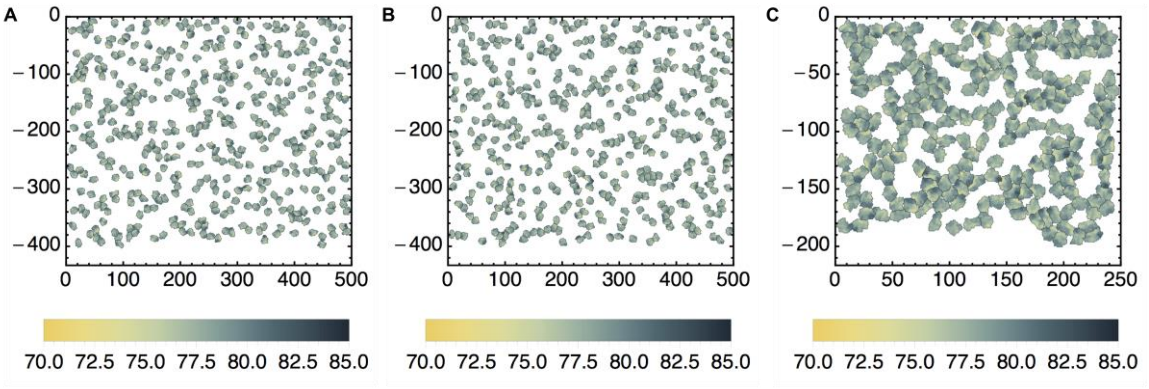

Figure 14 **Simulation of the endothelial tube formation process shows a directed, force-dependent migration.** (**A**) Control population after 1000 MCS. The simulation parameters were set as: Q_α=85, q_α=70, A=6, B=4, R_α=R_β=15, r_α=0.1, m_α=0.05, a_α=0.04, 400 cells, 2.5 x 10^5 lattice sites and non-periodic boundary conditions. (**B**) Chemotactic cell migration after 1000 MCS. Basic parameters identical to (A) and following chemotactic parameters: D=0.85, α=0.1, γ=0.35, K=10. (**C**) Mechanotransduction of directed migrating cells after 1000 MCS. Basic parameters identical to (A), mechanotransduction parameters: λ=100, d_{max}=50, 200 cells, 62 500 lattice sites and non-periodic boundary conditions (Parameters are defined in 7.2). *Simulations were performed by Andriy Goychuk.*

3.2 Comparative characterization of single endothelial cell migration in Matrigel and collagen I gels

3.2.1 Matrix composition influences morphology of migrating endothelial cells

To investigate if the matrix composition influences the migration phenotype of ECs, we embedded HUVECs in two structurally different hydrogels: Matrigel and rat tail collagen I. To visualize the topography of Matrigel we stained for its three major components, laminin, collagen type IV and the crosslinking protein entactin at different Matrigel concentrations. Here, we identified a dense gel with small pores (Figure 15A) and detected a correlation between the protein concentration and the mesh density of Matrigel. In contrast, collagen I staining (Figure 15B) showed a dense fibrillar network with a correlation between the fibrillar density and the protein concentration. We choose protein concentrations of the hydrogels, which resulted in comparable stiffness (Figure 15C). For the following experiments we used 2.49 mg/ml Matrigel and 1.00 mg/ml rat tail collagen I gels, since these concentrations resulted in the most reproducible migration

behavior of HUVECs. Interestingly, the cell morphology of HUVECs was completely different in both settings (Figure 15D). F-actin staining of HUVECs migrating in Matrigel showed an elongated cell shape, which is characterized by a lack of stress fibers, focal adhesions and a relatively thick cortical rim of f-actin, restricting the cell shape. We detected just very small blebs on the cell surface in HUVECs migrating in Matrigel. Additionally, HUVECs embedded in Matrigel (Figure 15D upper right panel) are characterized by a capping of ECM protein, shown here for collagen type IV. Furthermore, focusing on the gel topography, we observed persisting paths inside the gel, where the cell's route is reconstructable. These paths are coated with ECM proteins, here shown for collagen type IV. By contrast, HUVECs migrating in collagen I gels (Figure 15D bottom panel), showed a rounded cell shape with large blebs on the cell surface. We could not observe stress fibers or focal adhesions. Furthermore, immunostaining of collagen I revealed a protein coated cell surface. The cells are migrating along single collagen I fibers, paths are not detectable in contrast to cells migrating in Matrigel. Beside the round morphology we describe here for HUVECs migrating in collagen I gels, the cells temporary elongate during their migration cycle. Since we do not detect the rounded cell shape with pronounced blebs (diameter > 2 µm) in cells migrating in Matrigel, we compare this phenotype, characteristic for collagen I gels, to the elongated phenotype, predominantly detected in Matrigel.

As a measure of the physical hindrance that cells migrating in both settings have to overcome, we compared the cell migration velocity (Figure 15E): HUVECs migrating in collagen I gels are more than two times faster than cells migrating in Matrigel, independent of the concentration and the density of the gel. Thus the migration phenotype might mechanistically influence EC migration.

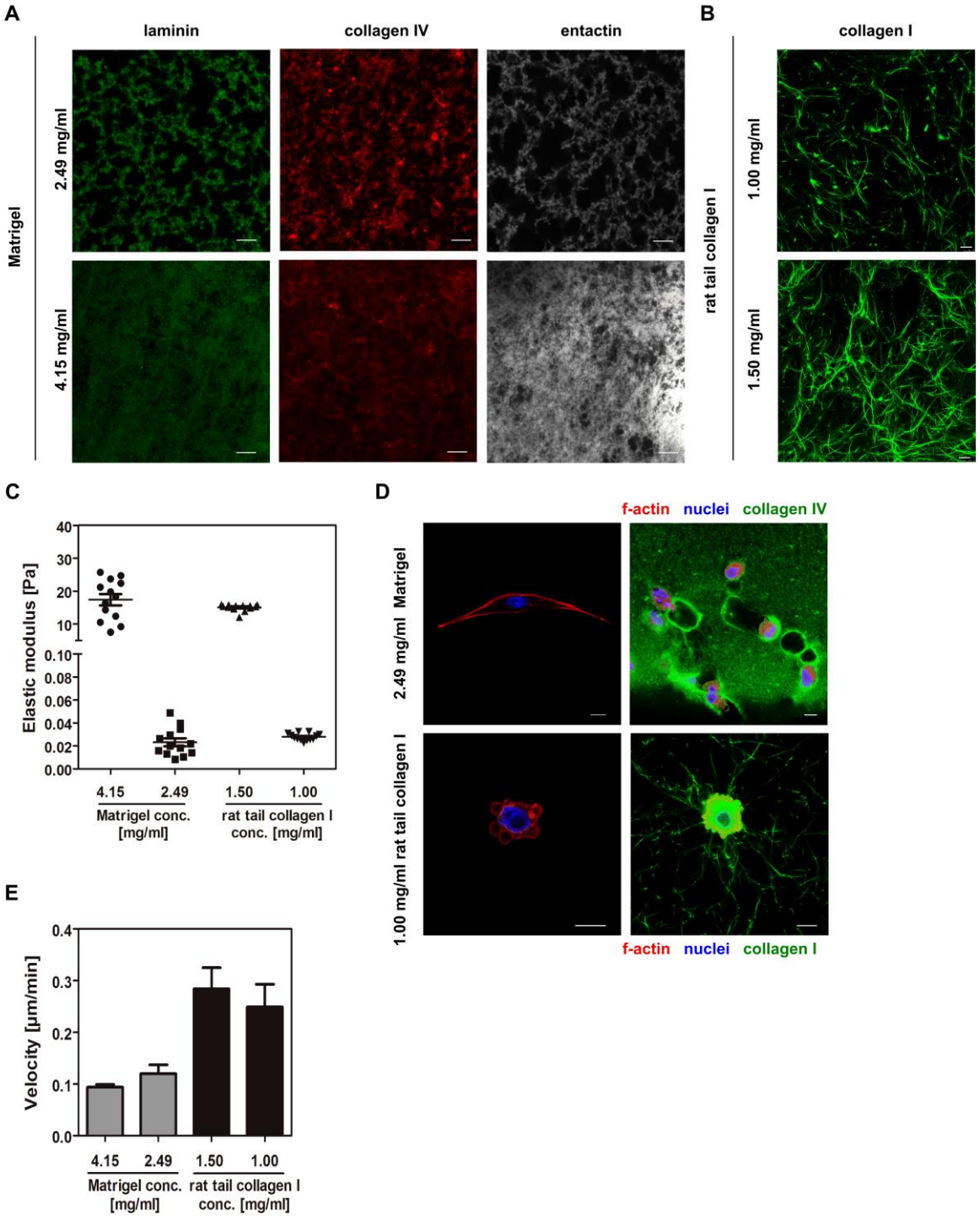

Figure 15 **Substrate topography influences morphology of ECs.** (**A**) Immunostaining of 4.15 mg/ml and 2.49 mg/ml sponge-like Matrigel, performed for laminin, collagen IV and entactin. (**B**) Confocal 3D view of collagen I staining in 1.50 mg/ml and 1.00 mg/ml fibrillar rat tail collagen I gels. (**C**) Determination of elastic modulus for Matrigel (4.15 and 2.49 mg/ml) and collagen I gels (1.50 and 1.00 mg/ml) by rheology. (**D**) Left, f-actin (red) and nuclei (blue) staining of elongated EC morphology in Matrigel and round EC shape in collagen I gel. Right, ECM proteins collagen I and IV were visualized by antibody staining (green). (**E**) Quantification of different cell migration velocities of HUVECs invading Matrigel or collagen I gels. HUVECs were migrating along a gradient of FCS (n=3). Bars, 10 µm.

3.2.2 The role of myosin II-dependent contractility depends on matrix composition

To investigate the effect of matrix composition on EC migration on a molecular level, we inhibited myosin II contractility in migrating HUVECs using blebbistatin. To quantify differences in migration behavior, we analyzed the FMI, directness and velocity of migrating HUVECs in Matrigel and collagen I gels (Figure 16A). To induce directed migration, we created a gradient of FCS (+/-). In order to distinguish between arbitrary migration effects and chemotaxis, we performed two reference measurements in all cases. For the negative control (-/-), we investigated the migration of cells in basal medium without chemoattractant, while as positive control (+/+), we filled the entire system with 10% FCS as chemoattractant, the control values should be below the FMI for directed migration. To indicate chemotaxis, the critical value of FMI, which discriminates between directed and non-directed migration is set at 0.1[63]. In Matrigel we observed no changes in velocity and chemotaxis after treatment with blebbistatin. In contrast, analyzing HUVECs migrating in collagen I gels, the FMI was significantly decreased compared to DMSO treated control cells, while the velocity of migrating cells was significantly increased after treatment with blebbistatin. To investigate whether the cell morphology is differently altered, too, we stained the f-actin of HUVECs migrating in Matrigel and collagen I gels (Figure 16B). Here we observed a switch from rounded mode with pronounced blebs in collagen I control cells to an elongated shape without blebs after treatment with blebbistatin. When cells were migrating in Matrigel they kept their elongated shape after treatment with blebbistatin. These observations were confirmed by quantification of cell morphology in both hydrogels (Figure 16C): HUVECs migrating in rat tail collagen I gels switched their mode from round pronounced blebs (84%) into elongated (88%) after treatment with blebbistatin, while HUVECs migrating in Matrigel kept their main elongated phenotype (69/85%). That implies, that inhibition of myosin II in collagen I gels induces a switch from the rounded bleb-based migration phenotype to the elongated mode, together with an increase in velocity and a decrease in the ability to sense the chemotactic gradient, while the migration of ECs in Matrigel remains unaffected.

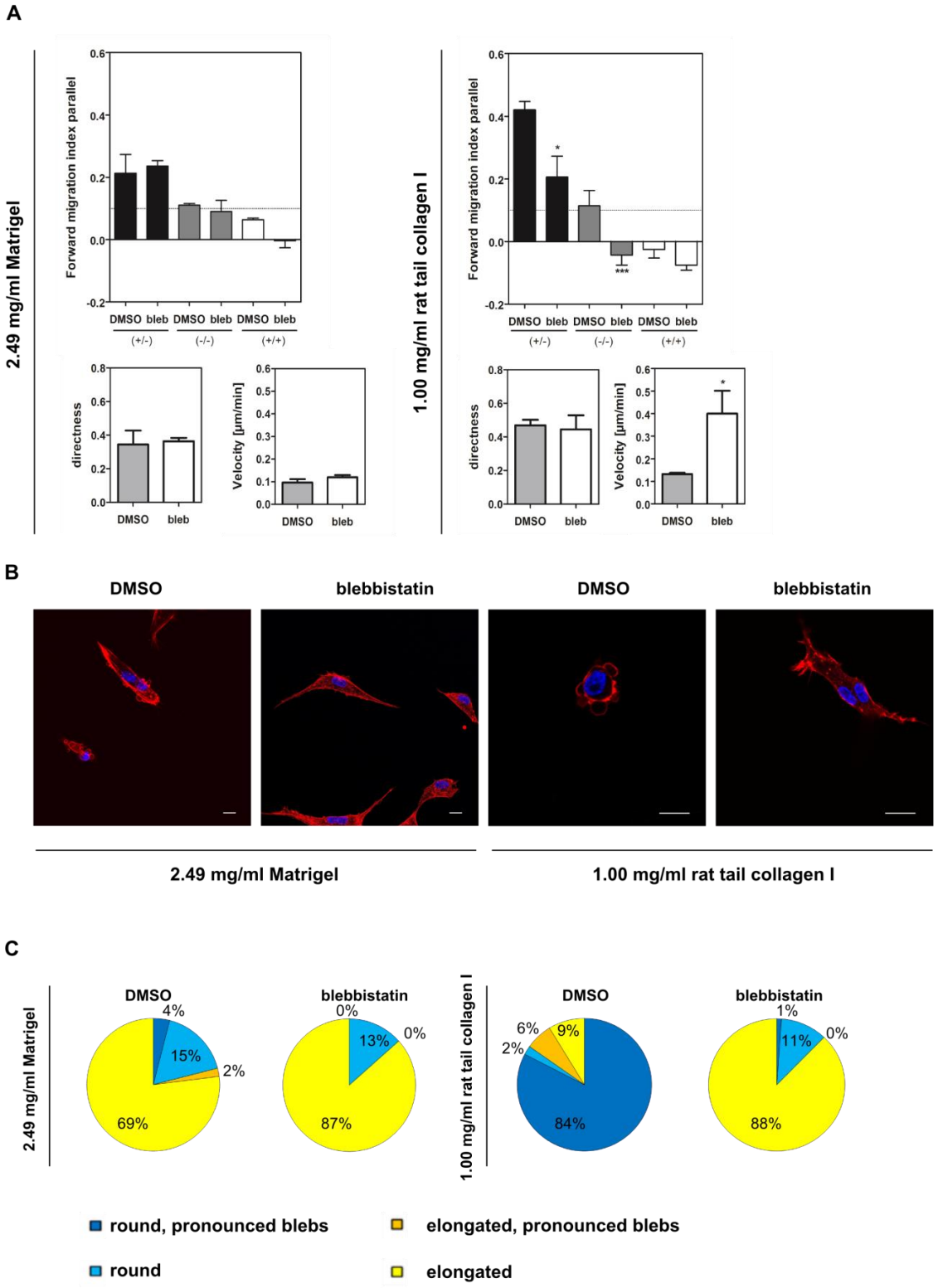

Figure 16 **Morphological and functional characterization of ECs in Matrigel and collagen I. (A)** Quantification of FMI in parallel to a chemotactic gradient, directness and velocity of ECs invading Matrigel or collagen I gels. Cells were treated with 10 µM blebbistatin (bleb) or DMSO as control. A FCS gradient was used to induce directed cell migration (+/-), additionally positive- (+/+), and negative- (-/-) controls were analyzed (n=3; *P≤0.05; ***P≤0.001). **(B)** F-actin (red) and nuclei (blue) staining of HUVECs showed a phenotypic switch after blebbistatin treatment in collagen I gels. **(C)** Quantification of cell morphology of HUVECs exemplarily shown in B (n=3). Bars, 10 µm.

3.2.3 Matrix composition influences polarization of small GTPases in endothelial cells

Beside contractility, we investigated the polarization of small GTPases as a further migration parameter. Here, immunostaining of Rac1 and Cdc42 showed different cellular localization of both proteins in Matrigel and collagen I gels (Figure 17A). In Matrigel both GTPases were distributed evenly all over the cell, while in collagen I Rac1 and Cdc42 showed a polarized localization in pronounced blebs at the leading edge of the cells. Analyzing quantitative parameters, the inhibition of Rac1 in Matrigel showed a significantly reduced FMI (Figure 17B), which was nevertheless higher than 0.1, implying chemotaxis. Since the directness of cells was unaffected, chemotaxis was not completely inhibited but restricted. In contrast, in collagen I gels chemotaxis was inhibited after treatment with the Rac1 inhibitor, shown by significant reduction of both, FMI and directness of cells. In this setting, the velocity of migration was significantly reduced, too. Using ML141, to inhibit Cdc42, we detected similar effects as for Rac1 inhibition: chemotaxis and the migration velocity were unaffected in Matrigel, while the FMI as well as the directness were significantly decreased in collagen I gels.

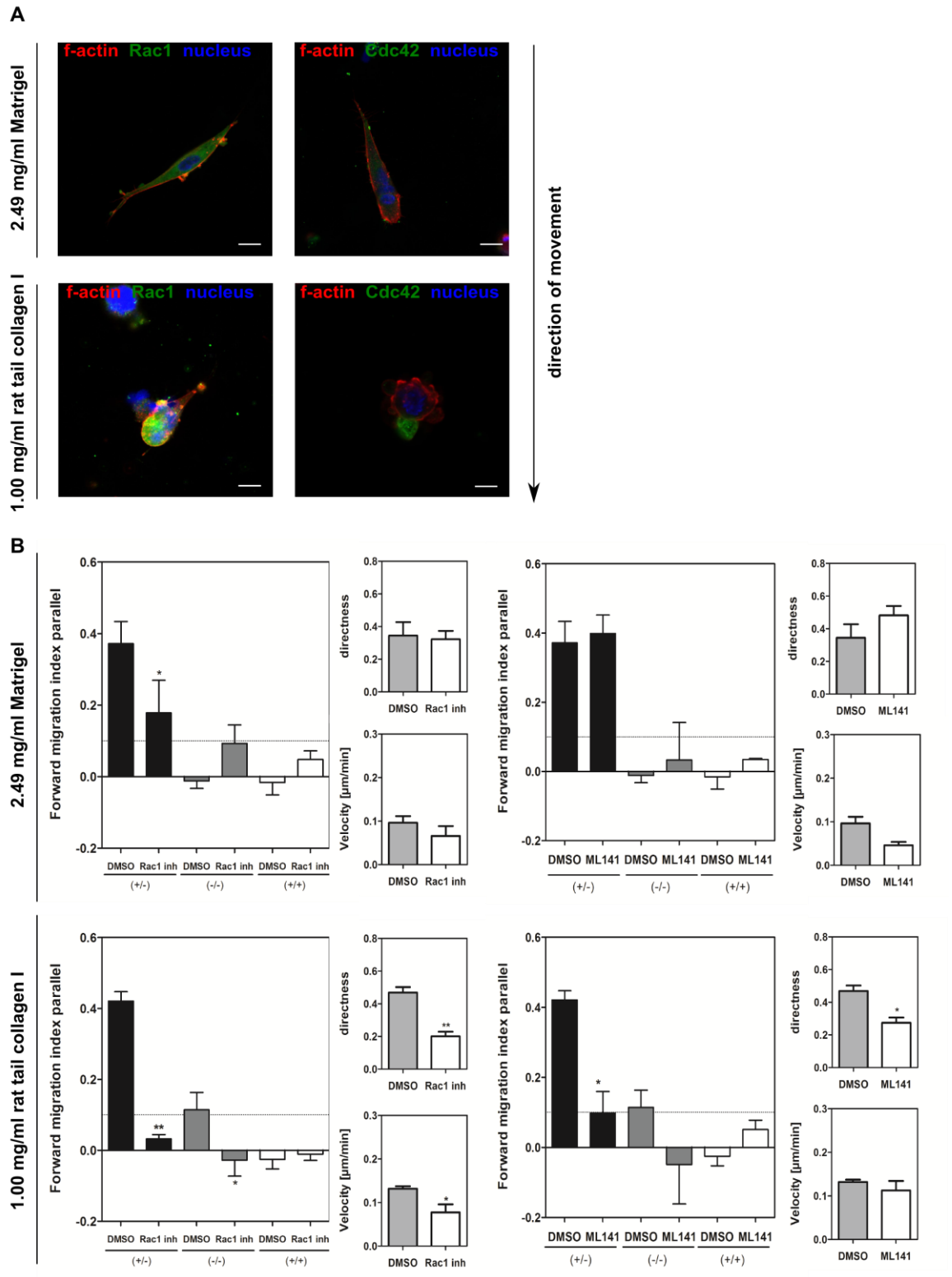

Figure 17 **Rac1 and Cdc42 as key-players in migration show different polarization-dependent effects in Matrigel and collagen I. (A)** Immunostaining of HUVECs invading Matrigel or collagen I gels for polarization markers Cdc42 and Rac1 (green), additionally f-actin (red) and nuclei (blue) were stained. The direction of movement was set by a FCS gradient. **(B)** Quantification of FMI in parallel to a chemotactic gradient, directness and velocity of HUVECs treated with 50 µM Rac1 inhibitor (Rac1 inh), 25 µM ML141 or DMSO, invading Matrigel or collagen I gels. FCS was used to induce directed cell migration (+/-), controls were analyzed as described in Figure 16 (n=3; *P≤0.05; **P≤0.01). Bars, 10 µm.

3.2.4 Self-secreted ECM proteins are deposited during migration in Matrigel and *in vivo*

To investigate whether matrix remodeling depends on the composition of the matrix, we stained for self-secreted proteins in Matrigel and collagen I. Here we could show that HUVECs deposit fibronectin during migration in Matrigel (Figure 18A). Fibronectin fibers were secreted to coat the paths, which were characteristically formed during migration in Matrigel (Figure 15D). To test whether the secreted fibronectin attaches to the cytoskeleton or the cell membrane, we performed f-actin staining and transfection of HUVECs with pMyrPalm_mEGFP, which is located at the cell membrane. We did not perform stainings of other ECM proteins like laminin and collagen IV, since these proteins are the main components of Matrigel and a clear distinction between self-secreted and matrix proteins would be not feasible. In collagen I gels staining of the ECM proteins fibronectin, laminin and collagen IV showed localization of these proteins on the cell surface but no deposition in the collagen matrix (Figure 18B). To investigate the relevance of self-secreted proteins *in vivo*, we performed staining of P3 mouse retina with an endothelial marker (isolectin GS-B_4, green) and immunostaining of the ECM protein laminin (red) (Figure 18C). This confirmed the deposition of laminin, as an exemplarily matrix protein, along newly built vessels *in vivo* in the mouse retina.

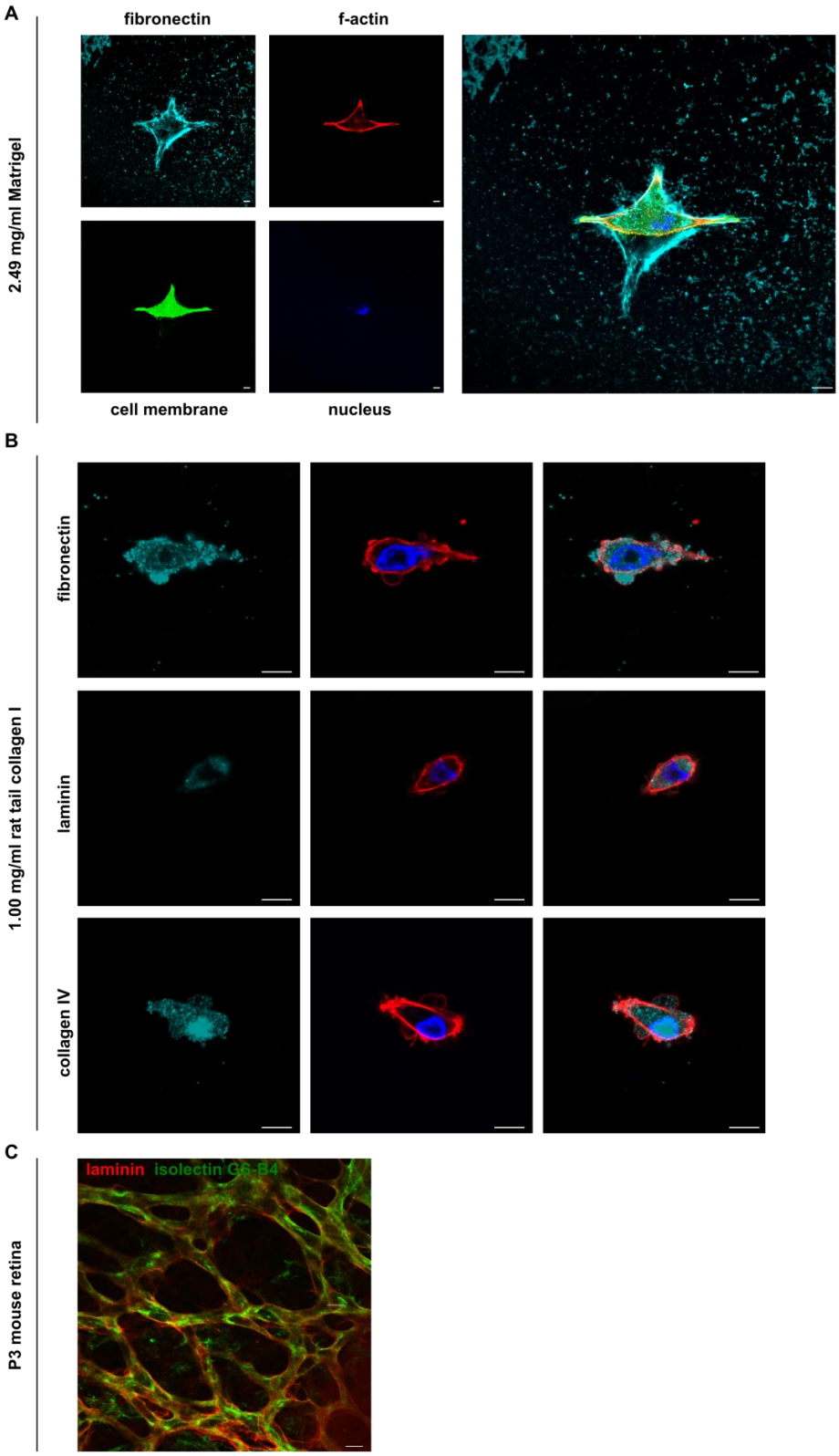

Figure 18 **ECs deposit ECM-proteins in Matrigel and in mouse retina tissue but not in collagen I gels**. **(A)** Confocal view of fibronectin (cyan) secreted and deposited by HUVECs invading Matrigel. Additionally visualization of cell membrane (green), f-actin (red) and nuclei (blue). **(B)** Confocal images of secreted fibronectin, laminin and collagen IV (cyan) of ECs invading collagen I gels. ECM proteins stick to the cell surface. **(C)** Laminin (red) deposition in P3 mouse retina. ECs (green) were stained with isolectin GS-B4. Bars, 10 µm.

3.2.5 Cell blebbing compensates for loss of proteolytic activity in collagen I gels

We showed differences in secretion and deposition of ECM proteins dependent on the environment of the cells (Figure 18). Therefore, we investigated the importance of proteolytic activity for the degradation of self-secreted ECM proteins for cells migrating in Matrigel (Figure 19A). To inhibit MMPs, we treated HUVECs with batimastat. The fluorescence intensity of laminin increased during the first 20 hours in DMSO treated control cells and decreased up to 70 hours afterwards. When cells were treated with batimastat, the secreted laminin was not degradable and the fluorescence intensity of laminin increased over the whole time period. To quantify the functional influence of MMP inhibition, we analyzed chemotaxis parameters as well as the velocity of migrating cells in Matrigel and collagen I gels (Figure 19B). Batimastat treatment of cells in Matrigel led to an inhibition of chemotaxis, while cell velocity of migrating cells was slightly increased. Whereas, both parameters were not influenced when cells were embedded into collagen I gels. To identify whether the ability to form pronounced cell blebs compensates the loss of proteolytic activity in collagen I gels, we induced the elongated phenotype, which is characteristic for cells migrating in Matrigel, by blebbistatin treatment and treated the cells additionally with batimastat (Figure 19C). This combinatory treatment of cells showed a significant loss of directed cell migration, while the velocity of cells was increased. These were exactly the same findings as we got for cells embedded in Matrigel (Figure 19B).

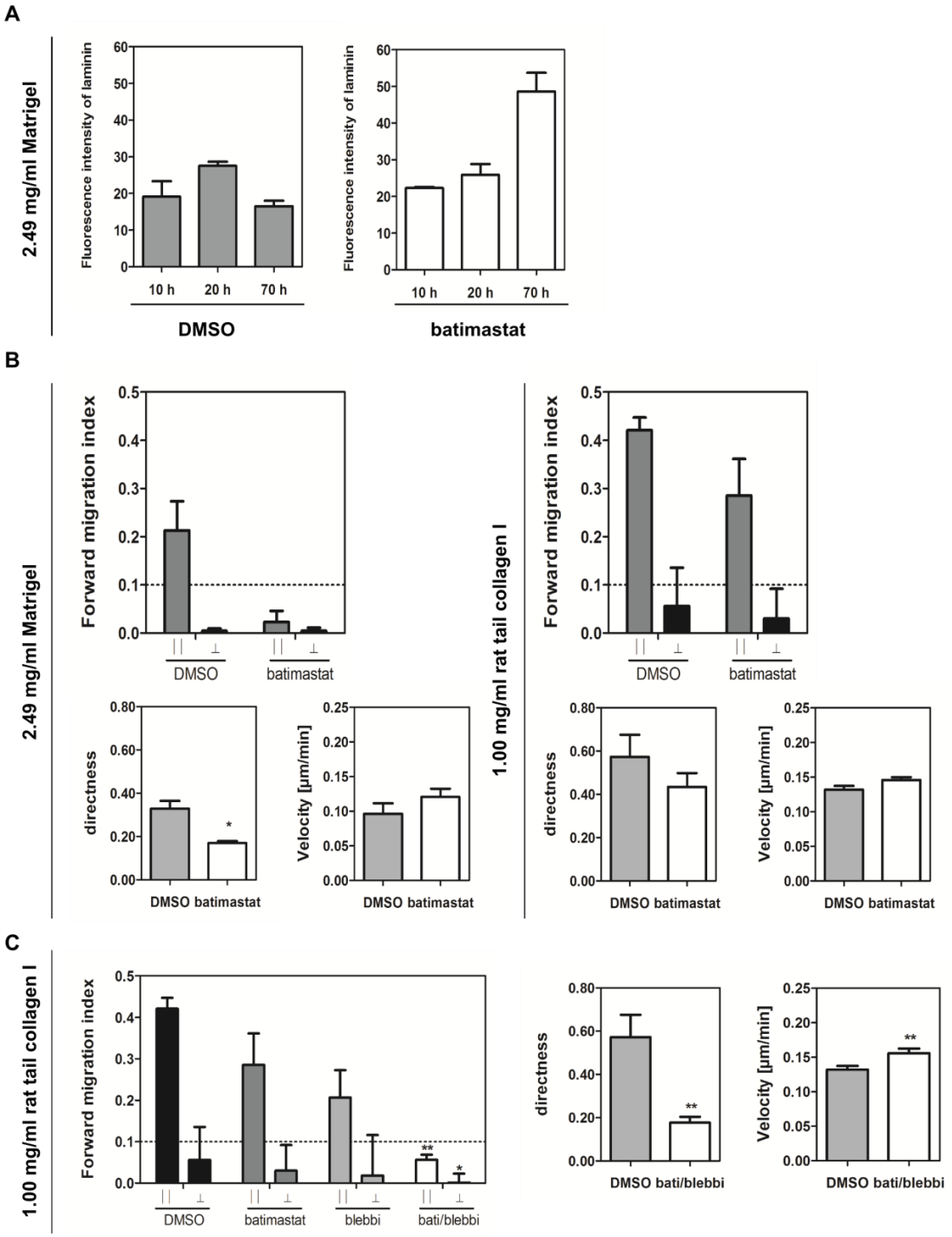

Figure 19 **Different effects of MMP inhibition in Matrigel and in collagen I gels. (A)** Quantification of fluorescence intensity of laminin after MMP inhibition by treatment with batimastat in Matrigel. The fluorescence intensity of laminin, which surrounded the cell surface, was analyzed using confocal images. HUVECs were fixed 10, 20 and 70 hours after embedding them into Matrigel. **(B)** Quantification of FMI in parallel and perpendicular to a chemotactic gradient, velocity and directness of HUVECs migrating in Matrigel and collagen I gels. MMPs were inhibited by treatment with 10 µM batimastat, DMSO was used as control. FCS was used as chemoattractant (n=3; *P≤0.05). **(C)** FMIs, directness and velocity of cells migrating in collagen I gels after treatment with 10 µM batimastat, 10 µM blebbistatin, and a combination of both (bati/blebbi), or DMSO as control. FCS was used as chemoattractant (n=3; *P≤0.05; **P≤0.001). Bars, 10 µm.

3.2.6 Inhibition of laminin binding integrins induces a morphological switch of endothelial cells

To address the question why HUVECs adapt a rounded morphology with pronounced blebbing in collagen I gels and not in Matrigel, we induced the formation of this mode in Matrigel by inhibition of different integrin-motifs (Figure 20A, B). Treatment of HUVECs migrating in Matrigel, with different α integrin antibodies showed that inhibition of laminin binding integrins (α_1, α_2, α_3, α_6) induced the formation of a rounded cell shape with pronounced blebs in Matrigel, representing a similar phenotype as seen in collagen I gels (Figure 15D). Inhibition of collagen and fibronectin binding integrins (α_4, α_5, α_v) did not change the elongated cell shape of migrating HUVECs compared to the control cells. Vice versa, we could show that addition of laminin to collagen I gels induced the elongated cell shape and inhibited pronounced cell blebbing (Figure 20C). Quantifying the cell migration velocity, we observed similar velocities of cells migrating in Matrigel and in collagen I gels supplemented with laminin. These velocities were significantly lower than the velocity of cells migrating in pure collagen I gels (Figure 20C).

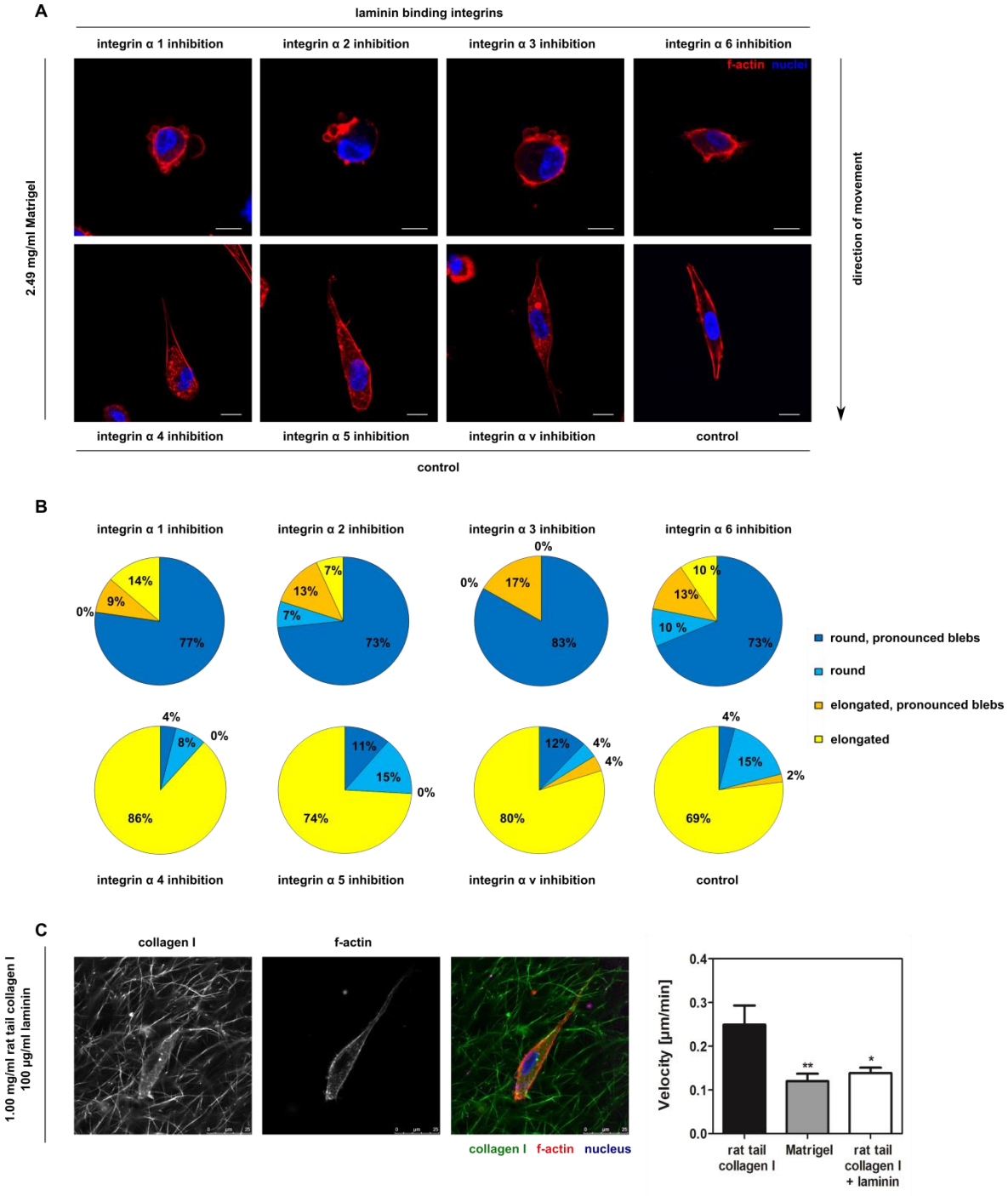

Figure 20 **Laminin determines elongated migration mode. (A)** F-actin (red) and nuclei (blue) staining of HUVECs invading Matrigel. Cell morphology was analyzed after inhibition of α1, 2, 3, 4, 5, 6 and v integrins by antibodies (40 µg/ml). A gradient of FCS guided the direction of movement. Bars, 10 µm. Based on these images, the cells were categorized into round with pronounced blebs (blebs > 2 µm), round, elongated with pronounced blebs and elongated **(B)**. At least 60 cells were analyzed. **(C)** Left panel, confocal view of HUVECs migrating in collagen I gels, supplemented with 100 µg/ml laminin. Collagen I was visualized by immunostaining, cells were stained for f-actin (red) and nuclei (blue). Right panel, quantification of cell migration velocity of HUVECs migrating in either collagen I gels, Matrigel or collagen I gels supplemented with laminin (n=3; *P≤0.05; **P≤0.01). Bars, 25 µm.

3.2.7 Endothelial cell migration *in vivo* approves elongated migration morphology, inhibition of laminin binding induces a morphological switch

To validate, which mode of migration resembles an *in vivo* situation of EC migration more closely, we established time-lapse live cell imaging of the growing vasculature of a P3 mouse retina expressing lifeact-EGFP (Figure 21A). 3D maximum intensity projection showed a smooth surface of the cells within the vascular network of the control retina (Figure 21A upper panel). Moreover, we could not detect any cell blebs or rounding of cells in the untreated retina, while inhibition of α_6 integrin induced extensive cell blebbing (Figure 21B bottom panel). Furthermore, we analyzed the cell shape of migrating cells, which build the leading front of the growing vasculature (Figure 21B). Here, we exclusively saw an elongated cell shape during the formation of vascular sprouts. The cells showed several filopodia located at the leading edge. In contrast, when the adhesion of cells to laminin was inhibited by an anti-α_6 integrin antibody, cell blebbing, as we observed during migration in collagen I gels, was detected. Thus, migration of ECs in murine retina resembles the elongated migration morphology, as observed in Matrigel (Figure 15D) and inhibition of laminin binding integrin α_6 leads to a morphological switch into the bleb-dependent migration phenotype.

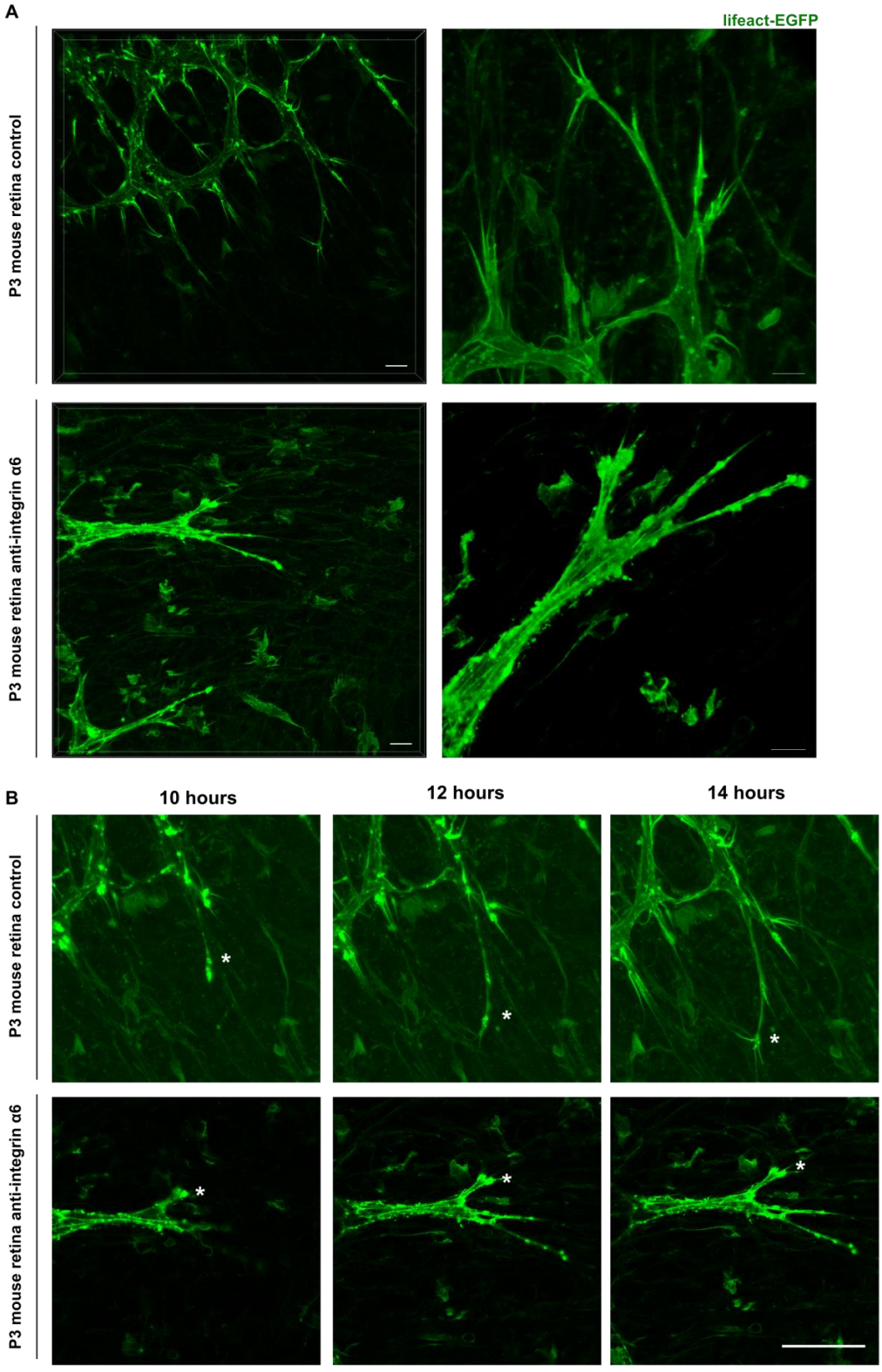

Figure 21 **Live-imaging of ECs in mouse retina shows elongated mode of migration *in vivo.*** (**A**) Confocal view of vasculature in P3 mouse retina, expressing Lifeact-EGFP in ECs. 3D maximum intensity projection was performed using IMARIS. Elongated morphology in the control retina (upper panel) switched into the blebbing based phenotype by treatment with an anti-integrin α_6 antibody (bottom panel). (**B**) Growing vasculature was imaged for 14 hours. Asterisks indicate the migration of elongated (upper panel) and blebbing (bottom panel) cells during vessel sprouting, 10, 12 and 14 hours after dissection of the retina. Bars, 10 µm.

4 DISCUSSION

4 DISCUSSION

4.1 Mechanical forces exerted on the matrix and matrix adhesion are decisive for endothelial tube formation

Angiogenesis is characterized by a complex morphogenetic cascade of events during which quiescent resting ECs become activated to proteolytically degrade their underlying ECM, directionally migrate towards the angiogenic stimulus, proliferate and align into new 3D capillary networks[4,66]. The EC tube formation on basement membranes encompasses all steps of the angiogenic process: adhesion, migration, alignment and tube formation. Hence, this assay has been widely used as a screen for angiogenic and anti-angiogenic factors[42,67]. Nevertheless, the mechanisms initiating EC tube formation on a basement membrane matrix, e.g. Matrigel, are mostly unknown. In this thesis it was possible to spatio-temporally characterize the process of endothelial tube formation. On the basis of experimental evidence and theoretical insights, we emphasize mechanical forces as main communication strategies for initiating cell-cell finding as well as matrix adhesion to be crucial for maturation of tubes *in vitro*.

4.1.1 Formation of initial cell-cell contacts is a directed process dependent on cell density

The results shown in this thesis indicate that cell density influences the initial communication of cells and hence, the formation of tubular structures. Too sparse cell density prohibits recognition of cells among themselves as well as tube formation. Consequently, the initial formation of cell-cell contacts seems to play a pivotal role for following tube maturation processes. Up to now initial cell finding was often assumed as a random process[68]. We used a mathematical model approach to validate this. Here we could show that endothelial tube formation is a directed process, which is not driven by chemotactic stimuli, like it is often hypothesized[69].

Most of the cell-based mathematical models of (tumor-induced) angiogenesis, available in literature, are modelling the angiogenic process without experimental basis[68,70,71]. In these models they often study blood vessel formation in relation to shear stress and pressure[72], or cell motion along gradients of chemical concentrations and adhesiveness[70]. Many studies rely on *in vivo* angiogenesis[70] or expect collagen as a well-characterized *in vitro* matrix[68]. Matrigel, which is often used for biological approaches investigating the

process of endothelial tube formation, is neglected in modelling studies up to now. An assumption, which is often made, is a random cell motion, where cells exert traction forces on the ECM. According to this hypothesis, the pulling of cells causes the ECM to move, and along with it the cells that have adhered to the moving gel. After a few hours, the cells are predicted to form aggregates and the ECM becomes reorganized: most of the ECM would then be accumulated underneath the cell clusters, while the remaining ECM has reorganized into a network of fibrous lines that tessellates the plane. These hypothetical lines have been postulated to be used by the cells as a scaffold for their migration[68]. Since we could show that ECs secret huge amounts of ECM proteins during migration, the assumed protein accumulations are not necessarily reorganized proteins but could also be self-secreted by the cells. Our study revealed that the forces exerted on the ECM are instead used to attract other cells and lead the way to the nearest neighbouring cell.

4.1.2 VEGF gradients are not inevitable for cell communication

Since during normal and pathological angiogenesis *in vivo*, gradients of secreted signalling proteins guide growing blood vessels[64], we considered chemotactic control of initial cell communication in the endothelial tube formation process. On the basis of the finding, that VEGF is known as a master switch of the angiogenic cascade at an early point in the hierarchical order of morphogenic events[73], 2D *in vitro* experiments have shown that stable VEGF gradients are sufficient for induction of EC chemotaxis[64]. Therefore, we investigated whether soluble or matrix bound gradients of VEGF are regulators for the initial communication of cells. We could show that (i) cell to matrix adhesion is critical for the formation as well as the maturation of tubules, (ii) although relatively large amounts of VEGF are secreted by ECs, matrix bound gradients of VEGF are not detectable, and (iii) soluble VEGF gradients are neither guiding the initial communication of cells, nor the formation of tubular structures.

Taken these observations together, another critical regulator for initial cell-cell communication has to exist.

4.1.3 Initial communication of cells depends on mechanical forces exerted on the substrate

There is evidence that cells exert forces via traction on their underlying substrate and that there is a link between the traction forces and the rigidity of the matrix.

It has been shown that slow moving cells such as fibroblasts exert forces via traction that are 100- to 1000-fold greater than it is necessary to propel the cells at normal speeds *in vitro*[74]. It is thought that such high levels of traction allow fibroblasts to compress and align ECM during repair of wounds[75] and during the development of dense connective tissues[76]. Furthermore it has been shown that NIH 3T3 fibroblasts generate stronger traction forces and spread to larger size on stiff substrates than on soft substrates[77]. This suggests that fibroblasts adaptively regulate their contractility in accord with the prevailing conditions of substrate stiffness.

The traction of ECs *in vitro* has been shown to be similar in magnitude to that of dermal fibroblasts[78]; therefore, it is plausible that ECs restructure ECM via traction for purposes of morphogenesis *in vivo*. The function of traction during angiogenesis is unclear; Vernon *et al*.[78] suggest that traction might contribute directly to the propulsion of ECs through ECM and/or facilitate the reorganization or clearance of ECM immediately ahead of invading ECs. ECs at the tips of adjacent sprouts would align ECM between them by a traction mediated two-center effect, and fuse to establish common lumen.

Our results investigating the early steps of tube formation on Matrigel, indicate that ECs communicate via traction forces they exert on the matrix. The displacement of fluorescent labelled microbeads showed that the cells actively deform their substrate. Furthermore, we could show that for low cell densities correlating with large distances between single cells, high substrate stiffness is necessary to create a field of deformation, which is large enough to bridge the gap between the cells. Using high cell densities (and thus low distances between single cells) the force transmission between cells is sufficient also on soft gels. This means with lower cell densities, the substrate has to get stiffer for effective transmission of cellular forces exerted on the substrate.

4.1.4 Laminin binding integrins might act as force sensors

Many biological processes, including angiogenesis depend on tightly controlled interactions between cells and the ECM. For traction-mediated interactions between ECs and ECM to occur, forces developed by the cytoskeleton must be transmitted across the plasma membrane to the ECM. Mediators of this process include the integrins, which link the actin-associated proteins, such as talin, vinculin and paxillin, to the ECM[79–81].

We used different integrin-blocking antibodies and could show that laminin is the crucial ECM protein, controlling EC tube formation. For the first time laminin has been shown to influence tube formation by Kubota *et al.*[82]. Of the 15 available laminin isoforms, laminin-1 has been shown to be of particular interest in angiogenesis, as it mediates EC adhesion and differentiation[83], tube formation and furthermore mediates the activity of

endostatin, an angiogenic inhibitor that blocks tube formation[84]. This laminin isoform is the major glycoprotein component of Matrigel[85]. It consists of a α1 chain, which contains an IKVAV (isoleucine, lysine, valine, alanine and valine) site which promotes collagenase, plasminogen and metalloproteinase activity[85–87]. The activation of these enzymes results in matrix degradation thereby permitting cellular detachment and migration, and the release of matrix-sequestered pro-angiogenic factors, all of which are central to tube formation[85].

There is evidence in literature that integrins themselves act as mechanosensors[88]. For instance, it has been shown that application of force to integrin $\alpha_5\beta_1$ is required for conversion to a state that can be chemically cross-linked to the fibronectin beneath a cell. Furthermore inhibition of cell contractility has been shown to block cross-linking but was rescued by application of force from fluid shear stress[89]. This indicates that laminin binding integrins might act as a force-sensor, which is crucial for initial cell communication by sensing mechanical forces exerted by neighbouring cells.

4.1.5 Cell adhesion and thus morphology of endothelial cells plays a pivotal role for the maturation of tubular structures

Mechanotransduction plays a critical role in cell motility, with actin fibers being the most important contractile components of the cytoskeleton that comprise bundles of actomyosin[12]. It has been shown that the stiffness of stress fibers can be altered by pharmacological perturbation of contractility: blebbistatin decreases the stiffness of stress fibers, while calyculin A increases it[90]. Mechanistic studies have shown that blebbistatin binds to myosin-ADP-P_i complex with a high affinity and interferes with the phosphate release process[91]. The alteration of stress fiber stiffness and thus the imbalance of contractility might be responsible for inhibition of tube formation after treatment of cells with blebbistatin. Connolly *et al.*[92] characterized the changes in cell shape, which are critical in EC tube formation. They have been shown that cells stimulated to form capillary tubes in the presence of Matrigel, disassemble their organized actin stress fibers and form dynamic protrusive structures, leading to capillary assembly. Consequently, the imbalance of actin stress fibers respectively contractility in this study might inhibit capillary assembly via hampering the formation of dynamic protrusive structures.

4.2 Endothelial cells switch their migration modes based on matrix composition

When Judah Folkman first presented the concept of starving a tumor by inhibiting angiogenesis, genetic stability and morphological homogeneity of ECs were postulated[7,93]. However, the migratory behavior of ECs has been mainly studied on 2D substrates. Though Blobel claimed that “3D trumps 2D when studying EC migration”[58], no detailed characterization of EC behavior in 3D exists up to now.

4.2.1 Matrix topography influences endothelial cell morphology

From different cell types we know that cell behavior depends on the dimensionality of the surrounding matrix[94], and its composition[95]. For example macrophages use either amoeboid migration mode in fibrillar collagen I or mesenchymal migration mode in Matrigel[96]. Additionally, for 3T3 cells it has been shown that substrate topography affects cell shape and migration by modifying cell-to-substrate interactions[97]. However, no such information on the migration of ECs exists. Here, we show that the morphology of migrating HUVECs is influenced by the surrounding matrix, too, but is basically different from fibroblasts or carcinoma cell lines[24]. HUVECs embedded into dense Matrigel display an elongated phenotype, with a thick rim of cortical actin. They deposit large amounts of ECM proteins presumably to stabilize their migration paths inside the gel. In fibrillar collagen I gels with a stiffness comparable to Matrigel the cells adapt a rounded cell shape with pronounced plasma membrane blebs, which resembles the amoeboid migration mode, which has been described for various cell types[24,98]. Up to now, cell blebbing in ECs was only investigated on 2D substrates, indicating a role of cellular blebs in the early stage of cell spreading[99]. The adaption of different cell morphologies might be necessary to compensate limiting substrate conditions, which enable or preclude migration in 3D ECM[22]. It should not be neglected that the nucleus is the largest single organelle in every cell[100]. Different matrix topographies and densities lead to compression of the nucleus, which induces alterations in gene expression[101], and thus, maybe also on the migration phenotype.

4.2.2 Bleb-driven migration in rat tail collagen I depends on contractility and polarization of small GTPases

Amoeboid cell migration has previously been found to be a fast mode of migration in dendritic and cancer cells as well as zebrafish embryos[102,103]. Cells migrating in this mode

have a dynamic actin cytoskeleton without stress fibers and the regulation of the actin cytoskeleton takes place via the small GTPases Rac, Rho and Cdc42. Characteristically, amoeboid cells show weak adhesions and contractility, which allows fast repolarization and turning[25]. HUVECs migrating in collagen I gels show a phenotype, which is similar to that of amoeboid cells, but interestingly the mechanisms of cell migration seem to be completely different. The myosin II inhibitor blebbistatin switches this “amoeboid-like” to an elongated morphology in collagen I gels with no effect on directed cell migration, while HUVECs migrating in an elongated morphology in Matrigel seem to be independent of contractility. Kolega[104] has shown that treatment of ECs with blebbistatin in a 2D setup inhibits cell migration. Consequently, the role of contractility depends on the dimensionality of the experiment as well as on the type of matrix, which is used. The inhibition of the polarization markers Rac1 and Cdc42 revealed that cells migrating in the elongated mode do not show a polarized distribution of Rac1 and Cdc42. In contrast, Rac1 and Cdc42 are localized in plasma membrane blebs in cells migrating in collagen I. In 2D experiments a clear polarization of HUVECs has been shown[105]. Treatment of cells with ML141[106] or the Rac1 inhibitor 553502[107] has been additionally shown to reduce directed cell migration in 2D settings. Here, we could also reveal differences in 3D compared to 2D. Moreover, a previous study has shown cell polarization in mesenchymal cells and unpolarized migration in amoeboid cells[108]. Thus, our findings indicate that the migration modes of HUVECs cannot be simply categorized into already existing models for tumor cells or fibroblasts and the migration phenotype strongly depends on the matrix.

4.2.3 Physiological remodeling of the ECM is absent in rat tail collagen I gels

The ECM is a highly dynamic structure, which constantly undergoes a remodeling process, where ECM components are deposited, degraded, or otherwise modified[109]. This is an important mechanism during cell differentiation, including processes such as angiogenesis and wound repair[110]. It has been shown that using a protease inhibitor mix to inhibit the matrix remodeling ability of mesenchymal cells induced mesenchymal to amoeboid transition[24]. HUVECs migrating in Matrigel deposit and assemble ECM proteins during migration, thus, they might compensate active degradation of the matrix, visible as small tunnels stabilizing the paths they dig inside the gel. However, in collagen I gels, the secreted ECM proteins stick to the cell surface but are not deposited in the matrix. The deposition of laminin around newly formed vessels in P3 mouse retina argues for a physiological relevance of deposited ECM proteins.

We could show that in Matrigel self-secreted ECM proteins that stick on the cell surface are degraded over time, which can be inhibited by batimastat. Treatment of HUVECs,

migrating in Matrigel with batimastat inhibits chemotaxis, and significantly diminishes the directness of cells, while the velocity stays surprisingly unaffected. This might be due to ECM proteins, which stick to the cell surface and prevent binding of the chemoattractant to its cell surface receptors. In collagen I gels, chemotaxis and velocity of migration are unaffected after batimastat treatment. The blebbing of cells, which occurs in collagen gels might compensate for the batimastat treatment: blebbing might increase the cell surface and thus keep the ability to recognize chemotactic stimuli. In a previous study it has been indicated that inhomogeneity in membrane curvature affects protein association[111]. We confirmed the role of membrane blebbing in this context by combinatory treatment of cells with batimastat and blebbistatin in collagen I gels.

4.2.4 Laminin determines the migration mode

The role of laminin in angiogenic processes has been previously shown[112]. Adhesion of ECs to laminin has been described to induce Dll4 expression and thus leads to an activation of the Notch pathway. Dll4/Notch participates in the establishment of an adequate balance between tip and stalk cells during angiogenic sprouting. Additionally, appropriate laminin/integrin-induced signaling has been shown to be essential to induce physiologically functional levels of Dll4 expression and regulate the branching frequency during angiogenesis *in vivo*[113]. By the inhibition of laminin binding integrins, we could on the one hand induce a round bleb-based migration phenotype in Matrigel, which we otherwise only detected in collagen I gels. On the other hand, addition of laminin to collagen I gels in concentrations, which were shown to have no influence on the stiffness of the hydrogel[114], induced a switch from the usually rounded bleb-based migration mode to an elongated cell phenotype. Hence, we assume laminin as the main determinant of the migration mode of HUVECs.

4.2.5 Physiological migration of endothelial cells in mouse retina is similar to elongated migration morphology in Matrigel

In vivo EC migration is often studied in zebrafish[115–117]. In this model optical resolution imaging of the vasculature in developing animals over time has been established. Nevertheless, the relevance of fish EC angiogenesis is under debate[8]. To our knowledge, there is no mammalian model for angiogenesis, which allows life-imaging of the growing vasculature. Our murine retina model shows the behavior of ECs during the formation of new vessels. ECs are migrating in an elongated shape with no visible rounding or surface blebbing. A 3D image rendering shows relatively smooth cell surfaces. We could clearly

identify a tip and stalk cell phenotype of ECs[14]. The cells do not move as a sheet but form sprouts in the direction of movement. The retina model can be related to our single cell migration study, since the single cells obviously phenotypically mimic tip cell characteristics. Apart from that, inhibition of α_6 integrin in the murine retina induced a switch from the elongated phenotype into extensive blebbing on the cell surface. This validates our findings about the importance of laminin as the main determinant of the migration mode.

4.3 Conclusion and future perspectives

This study demonstrates that early stages of endothelial tube formation are controlled by mechanotransduction, with laminin binding integrins acting as force sensors. Furthermore, focusing on the migration of single cells, an enormous contextual plasticity of ECs is shown. The cells are able to switch between an elongated cell shape, ordinarily detected in spongy Matrigel and a round morphology with pronounced cell blebs, depicted in fibrillar collagen I gels and use this shift to evade pharmacological inhibition of contractility, small GTPases and proteolysis.

This is a long stride towards a better understanding of EC migration in 3D model systems as well as of the tube formation process, to further close the gap between *in vitro* approaches and *in vivo* models of angiogenesis. Based on these findings a directed manipulation of hydrogels might be possible to create a new dimension of angiogenic model systems, mimicking the processes *in vivo* more closely.

5 SUMMARY

5 SUMMARY

Angiogenesis, the formation of a vascular network originating from already existing vessels, is of persistent and central interest for both, developmental and pathological processes. Judah Folkman was the first, who presented the concept of starving a tumor by inhibiting angiogenesis[7]. In this early study of angiogenesis, he postulated a high genetic stability and morphological homogeneity of ECs. Further studies mainly investigated the behavior of ECs on flat 2D substrates and up to now there is still a large gap between classical *in vitro* approaches, which are easy to handle, but have a low prognostic value, and elaborated *in vivo* models, which facilitate a closer look at the reality, but allow only a low degree of spatio-temporal control[118].

In this work we spatio-temporally characterized endothelial tube formation on Matrigel and identified a close interaction between biophysical and cell biological parameters.

Here, we show that initial phases of endothelial tube formation are independent of chemotaxis, more precisely soluble or matrix bound gradients of VEGF. Further we depict the influence of cell to cell distances, which are decisive for the recognition of cells. Additionally, there is coherence between cell density and the rigidity of the matrix. Since cells actively deform their underlying substrate by exerting mechanical forces, with an important role of contractility, we concluded that the initial formation of cell-cell contacts, the first step of endothelial tube formation, is driven by mechanotaxis. Here, laminin binding integrins might act as important sensors for mechanical forces.

To understand morphogenetic systems such as the vasculature and depict its heterogeneity, it is inevitable to additionally consider the vessels as composed of autonomous, individual entities, in this case single ECs.

Therefore, we characterize the migration of single ECs through two structurally different hydrogels: spongy Matrigel and fibrillar collagen I. ECs adapt an elongated migration morphology in Matrigel, and a rounded cell shape with pronounced cell blebs (blebs > 2 µm) in collagen I, with laminin as the main determinant of the elongated phenotype, which facilitates a morphological switch between these modes. Further, we feature that ECs can evade pharmacological inhibition of contractility, small GTPases and proteolysis by morphological switches between these two modes. As *in-situ* proof of principle, we established live-imaging of EC migration during vascular growth in a murine retina, which reveals an elongated phenotype in untreated retina and a shift into extensive cell blebbing after inhibition of integrin binding to laminin.

Concluding, this work provides evidence for an unexpected contextual plasticity of EC behavior in 3D matrices and reveals the importance of mechanotransduction in angiogenesis.

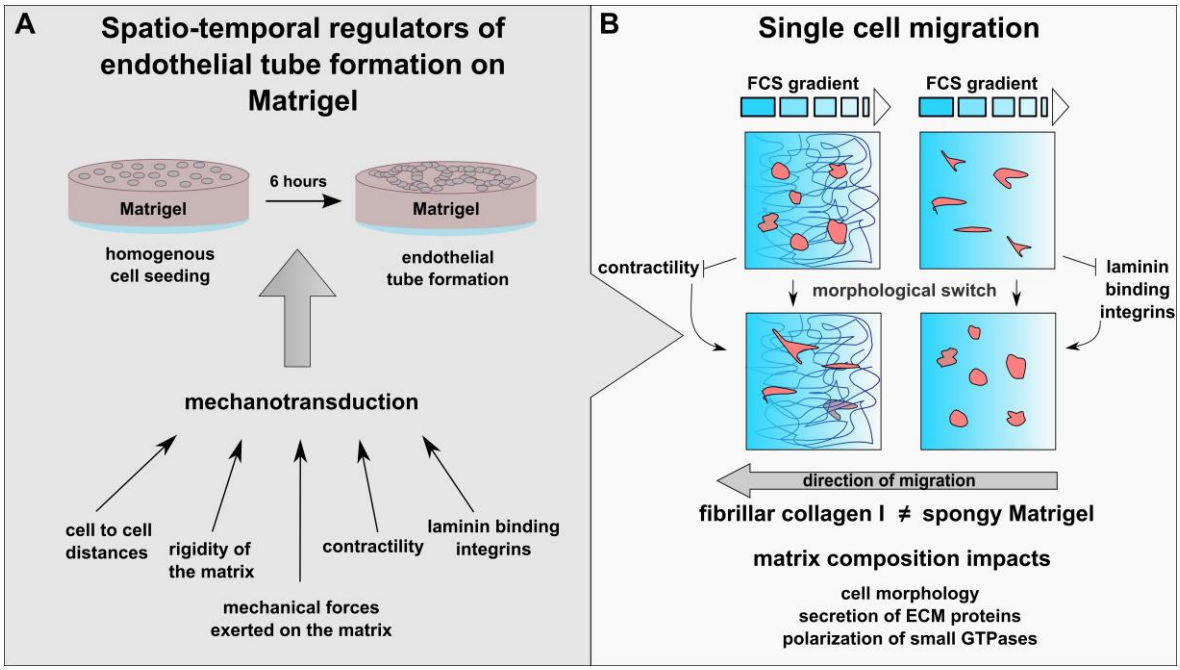

Figure 22 **Summary of the thesis.** (**A**) Spatio-temporal characterization of endothelial tube formation on Matrigel reveals mechanotransduction as the main regulator of early stages of tubule formation. Cell to cell distances, matrix rigidity, mechanical forces exerted on the matrix, contractility and laminin binding integrins influence the process. (**B**) On single cell level the composition of the matrix regulates cell morphology, secretion of matrix proteins and the polarization of small GTPases. Endothelial cells show a round phenotype in collagen I gels, which is switched into an elongated migration mode according to inhibition of contractility. In contrast cells show an elongated cell shape in Matrigel which shifts to the rounded shape by blocking of integrin binding to laminin.

6 REFERENCES

6 REFERENCES

1. Vailhé, B. Vittet, D. & Feige, J. J. In vitro models of vasculogenesis and angiogenesis, *Laboratory investigation; a journal of technical methods and pathology* 81, 439–452 (2001).

2. Lamalice, L. Le Boeuf, F. & Huot, J. Endothelial cell migration during angiogenesis, *Circulation research* 100, 782–794 (2007).

3. Risau, W. & Flamme, I. Vasculogenesis, *Annual review of cell and developmental biology* 11, 73–91 (1995).

4. Risau, W. Mechanisms of angiogenesis, *Nature* 386, 671–674 (1997).

5. Rousseau, S. Houle, F. Landry, J. & Huot, J. p38 MAP kinase activation by vascular endothelial growth factor mediates actin reorganization and cell migration in human endothelial cells, *Oncogene* 15, 2169–2177 (1997).

6. Potente, M. Gerhardt, H. & Carmeliet, P. Basic and therapeutic aspects of angiogenesis, *Cell* 146, 873–887 (2011).

7. Folkman, J. Tumor angiogenesis: therapeutic implications, *N. Engl. J. Med.* 285, 1182–1186 (1971).

8. Staton, C. A. Reed, Malcolm W R & Brown, N. J. A critical analysis of current in vitro and in vivo angiogenesis assays, *International journal of experimental pathology* 90, 195–221 (2009).

9. Lawson, N. D. *et al.* Notch signaling is required for arterial-venous differentiation during embryonic vascular development, *Development (Cambridge, England)* 128, 3675–3683 (2001).

10. Müller, A. M. Hermanns, M. I. Cronen, C. & Kirkpatrick, C. J. Comparative study of adhesion molecule expression in cultured human macro- and microvascular endothelial cells, *Experimental and molecular pathology* 73, 171–180 (2002).

11. Carson-Walter, E. B. *et al.* Cell surface tumor endothelial markers are conserved in mice and humans, *Cancer research* 61, 6649–6655 (2001).

12. Kaur, S. *et al.* RhoJ/TCL regulates endothelial motility and tube formation and modulates actomyosin contractility and focal adhesion numbers, *Arteriosclerosis, thrombosis, and vascular biology* 31, 657–664 (2011).

13. Jaffe, E. A. Nachman, R. L. Becker, C. G. & Minick, C. R. Culture of human endothelial cells derived from umbilical veins. Identification by morphologic and immunologic criteria, *The Journal of clinical investigation* 52, 2745–2756 (1973).

14. Smet, F. de, Segura, I. Bock, K. de, Hohensinner, P. J. & Carmeliet, P. Mechanisms of vessel branching: filopodia on endothelial tip cells lead the way, *Arteriosclerosis, thrombosis, and vascular biology* 29, 639–649 (2009).

15. Gerhardt, H. *et al.* VEGF guides angiogenic sprouting utilizing endothelial tip cell filopodia, *The Journal of cell biology* 161, 1163–1177 (2003).

16. Siekmann, A. F. & Lawson, N. D. Notch signalling limits angiogenic cell behaviour in developing zebrafish arteries, *Nature* 445, 781–784 (2007).

17. Gerhardt, H. *et al.* Neuropilin-1 is required for endothelial tip cell guidance in the developing central nervous system, *Developmental dynamics : an official publication of the American Association of Anatomists* 231, 503–509 (2004).

18. Suchting, S. *et al.* The Notch ligand Delta-like 4 negatively regulates endothelial tip cell formation and vessel branching, *Proceedings of the National Academy of Sciences of the United States of America* 104, 3225–3230 (2007).

19. Ruhrberg, C. *et al.* Spatially restricted patterning cues provided by heparin-binding VEGF-A control blood vessel branching morphogenesis, *Genes & development* 16, 2684–2698 (2002).

20. Blanco, R. & Gerhardt, H. VEGF and Notch in tip and stalk cell selection, *Cold Spring Harbor perspectives in medicine* 3, a006569 (2013).

21. Baker, B. M. & Chen, C. S. Deconstructing the third dimension: how 3D culture microenvironments alter cellular cues, *Journal of cell science* 125, 3015–3024 (2012).

22. Wolf, K. *et al.* Physical limits of cell migration: control by ECM space and nuclear deformation and tuning by proteolysis and traction force, *The Journal of cell biology* 201, 1069–1084 (2013).

23. Petrie, R. J. Gavara, N. Chadwick, R. S. & Yamada, K. M. Nonpolarized signaling reveals two distinct modes of 3D cell migration, *The Journal of cell biology* 197, 439–455 (2012).

24. Wolf, K. *et al.* Compensation mechanism in tumor cell migration: mesenchymal–amoeboid transition after blocking of pericellular proteolysis, *The Journal of cell biology* 160, 267–277 (2003).

25. Lämmermann, T. & Sixt, M. Mechanical modes of 'amoeboid' cell migration, *Current opinion in cell biology* 21, 636–644 (2009).

26. Lewis, W. H. Observations on cells in tissue-cultures with dark-field illumination, *Anat. Rec.* 26, 15–29 (1923).

27. Coleman, M. L. *et al.* Membrane blebbing during apoptosis results from caspase-mediated activation of ROCK I, *Nature cell biology* 3, 339–345 (2001).

28. Shiratsuchi, A. Mori, T. & Nakanishi, Y. Independence of plasma membrane blebbing from other biochemical and biological characteristics of apoptotic cells, *The Journal of Biochemistry* 132, 381–386 (2002).

29. Fackler, O. T. & Grosse, R. Cell motility through plasma membrane blebbing, *The Journal of cell biology* 181, 879–884 (2008).

30. Ridley, A. J. Rho GTPase signalling in cell migration, *Current opinion in cell biology* 36, 103–112 (2015).

31. Boureux, A. Vignal, E. Faure, S. & Fort, P. Evolution of the Rho Family of Ras-Like GTPases in Eukaryotes, *Molecular Biology and Evolution* 24, 203–216 (2006).

32. Tal, O. *et al.* DC mobilization from the skin requires docking to immobilized CCL21 on lymphatic endothelium and intralymphatic crawling, *Journal of Experimental Medicine* 208, 2141–2153 (2011).

33. Montell, D. J. Yoon, W. H. & Starz-Gaiano, M. Group choreography. Mechanisms orchestrating the collective movement of border cells, *Nat Rev Mol Cell Biol* 13, 631–645 (2012).

34. Machacek, M. *et al.* Coordination of Rho GTPase activities during cell protrusion, *Nature* 461, 99–103 (2009).

35. Wu, C. *et al.* Arp2/3 Is Critical for Lamellipodia and Response to Extracellular Matrix Cues but Is Dispensable for Chemotaxis, *Cell* 148, 973–987 (2012).

36. Charras, G. & Paluch, E. Blebs lead the way: how to migrate without lamellipodia, *Nature reviews. Molecular cell biology* 9, 730–736 (2008).

37. Folkman, J. & Haudenschild, C. Angiogenesis in vitro, *Nature* 288, 551–556 (1980).

38. Ingber, D. E. & Folkman, J. How does extracellular matrix control capillary morphogenesis?, *Cell* 58, 803–805 (1989).

39. Pelletier, L. Regnard, J. Fellmann, D. & Charbord, P. An in vitro model for the study of human bone marrow angiogenesis: role of hematopoietic cytokines, *Laboratory investigation; a journal of technical methods and pathology* 80, 501–511 (2000).

40. Kalluri, R. Basement membranes: structure, assembly and role in tumour angiogenesis, *Nature reviews. Cancer* 3, 422–433 (2003).

41. Hallmann, R. *et al.* Expression and function of laminins in the embryonic and mature vasculature, *Physiological reviews* 85, 979–1000 (2005).

42. Auerbach, R. Lewis, R. Shinners, B. Kubai, L. & Akhtar, N. Angiogenesis assays: a critical overview, *Clinical chemistry* 49, 32–40 (2003).

43. Azad, A. K. Sermsintham, N. Chandrkrachang, S. & Stevens, W. F. Chitosan membrane as a wound-healing dressing: characterization and clinical application, *Journal of biomedical materials research. Part B, Applied biomaterials* 69, 216–222 (2004).

44. Lysaght, M. J. & Aebischer, P. Encapsulated cells as therapy, *Scientific American* 280, 76–82 (1999).

45. Lee, K. Y. & Mooney, D. J. Hydrogels for tissue engineering, *Chemical reviews* 101, 1869–1879 (2001).

46. Wang, C. Stewart, R. J. & Kopecek, J. Hybrid hydrogels assembled from synthetic polymers and coiled-coil protein domains, *Nature* 397, 417–420 (1999).

47. Petka, W. A. Harden, J. L. McGrath, K. P. Wirtz, D. & Tirrell, D. A. Reversible hydrogels from self-assembling artificial proteins, *Science (New York, N.Y.)* 281, 389–392 (1998).

48. Hughes, C. S. Postovit, L. M. & Lajoie, G. A. Matrigel: a complex protein mixture required for optimal growth of cell culture, *Proteomics* 10, 1886–1890 (2010).

49. Kleinman, H. K. & Martin, G. R. Matrigel: basement membrane matrix with biological activity, *Seminars in Cancer Biology* 15, 378–386 (2005).

50. Kleinman, H. K. *et al.* Isolation and characterization of type IV procollagen, laminin, and heparan sulfate proteoglycan from the EHS sarcoma, *Biochemistry* 21, 6188–6193 (1982).

51. Orkin, R. W. *et al.* A murine tumor producing a matrix of basement membrane, *The Journal of experimental medicine* 145, 204–220 (1977).

52. Segev, A. Nili, N. & Strauss, B. H. The role of perlecan in arterial injury and angiogenesis, *Cardiovascular research* 63, 603–610 (2004).

53. Schéele, S. *et al.* Laminin isoforms in development and disease, *Journal of molecular medicine (Berlin, Germany)* 85, 825–836 (2007).

54. Miner, J. H. Laminins and their roles in mammals, *Microscopy research and technique* 71, 349–356 (2008).

55. Suzuki, N. Yokoyama, F. & Nomizu, M. Functional sites in the laminin alpha chains, *Connective tissue research* 46, 142–152 (2005).

56. Bonnefoy, A. Moura, R. & Hoylaerts, M. F. The evolving role of thrombospondin-1 in hemostasis and vascular biology, *Cellular and molecular life sciences : CMLS* 65, 713–727 (2008).

57. Carmeliet, P. Angiogenesis in life, disease and medicine, *Nature* 438, 932–936 (2005).

58. Blobel, C. P. 3D trumps 2D when studying endothelial cells, *Blood* 115, 5128–5130 (2010).

59. Riedl, J. *et al.* Lifeact mice for studying F-actin dynamics, *Nature methods* 7, 168–169 (2010).

60. Fraccaroli, A. *et al.* Visualization of endothelial actin cytoskeleton in the mouse retina, *PloS one* 7, e47488 (2012).

61. Niwa, H. Yamamura, K.-i. & Miyazaki, J.-i. Efficient selection for high-expression transfectants with a novel eukaryotic vector, *Gene* 108, 167–321 (1991).

62. Sawamiphak, S. Ritter, M. & Acker-Palmer, A. Preparation of retinal explant cultures to study ex vivo tip endothelial cell responses, *Nature protocols* 5, 1659–1665 (2010).

63. Zengel, P. *et al.* µ-Slide Chemotaxis: a new chamber for long-term chemotaxis studies, *BMC cell biology* 12, 21 (2011).

64. Barkefors, I. *et al.* Endothelial cell migration in stable gradients of vascular endothelial growth factor A and fibroblast growth factor 2: effects on chemotaxis and chemokinesis, *The Journal of biological chemistry* 283, 13905–13912 (2008).

65. Pepper, M. S. Role of the Matrix Metalloproteinase and Plasminogen Activator-Plasmin Systems in Angiogenesis, *Arteriosclerosis, thrombosis, and vascular biology* 21, 1104–1117 (2001).

66. Augustin, H. G. Antiangiogenic tumour therapy: will it work?, *Trends in pharmacological sciences* 19, 216–222 (1998).

67. Browning, A. C. Dua, H. S. & Amoaku, W. M. The effects of growth factors on the proliferation and in vitro angiogenesis of human macular inner choroidal endothelial cells, *The British journal of ophthalmology* 92, 1003–1008 (2008).

68. Manoussaki, D. A mechanochemical model of angiogenesis and vasculogenesis, *ESAIM: M2AN* 37, 581–599 (2003).

69. Serini, G. *et al.* Modeling the early stages of vascular network assembly, *The EMBO journal* 22, 1771–1779 (2003).

70. Bauer, A. L. Jackson, T. L. & Jiang, Y. A cell-based model exhibiting branching and anastomosis during tumor-induced angiogenesis, *Biophysical journal* 92, 3105–3121 (2007).

71. Holmes, M. J. & Sleeman, B. D. A mathematical model of tumour angiogenesis incorporating cellular traction and viscoelastic effects, *Journal of theoretical biology* 202, 95–112 (2000).

72. Gödde, R. & Kurz, H. Structural and biophysical simulation of angiogenesis and vascular remodeling, *Developmental dynamics : an official publication of the American Association of Anatomists* 220, 387–401 (2001).

73. Augustin, H. G. Tubes, branches, and pillars: the many ways of forming a new vasculature, *Circulation research* 89, 645–647 (2001).

74. Harris, A. K. Stopak, D. & Wild, P. Fibroblast traction as a mechanism for collagen morphogenesis, *Nature* 290, 249–251 (1981).

75. Stopak, D. & Harris, A. K. Connective tissue morphogenesis by fibroblast traction. I. Tissue culture observations, *Developmental Biology* 90, 383–398 (1982).

76. Reed, M. J. Vernon, R. B. Abrass, I. B. & Sage, E. H. TGF-beta 1 induces the expression of type I collagen and SPARC, and enhances contraction of collagen

gels, by fibroblasts from young and aged donors, *Journal of cellular physiology* 158, 169–179 (1994).

77. Lo, C. M. Wang, H. B. Dembo, M. & Wang, Y. l. Cell movement is guided by the rigidity of the substrate, *Biophysical journal* 79, 144–152 (2000).

78. Vernon, R. B. & Sage, E. H. Between molecules and morphology. Extracellular matrix and creation of vascular form, *The American journal of pathology* 147, 873–883 (1995).

79. Beckerle, M. C. & Yeh, R. K. Talin: role at sites of cell-substratum adhesion, *Cell motility and the cytoskeleton* 16, 7–13 (1990).

80. Otey, C. A. Pavalko, F. M. & Burridge, K. An interaction between alpha-actinin and the beta 1 integrin subunit in vitro, *The Journal of cell biology* 111, 721–729 (1990).

81. Turner, C. E. Glenney, J. R. & Burridge, K. Paxillin: a new vinculin-binding protein present in focal adhesions, *The Journal of cell biology* 111, 1059–1068 (1990).

82. Kubota, Y. Role of laminin and basement membrane in the morphological differentiation of human endothelial cells into capillary-like structures, *The Journal of cell biology* 107, 1589–1598 (1988).

83. Dixelius, J. *et al.* Laminin-1 promotes angiogenesis in synergy with fibroblast growth factor by distinct regulation of the gene and protein expression profile in endothelial cells, *The Journal of biological chemistry* 279, 23766–23772 (2004).

84. Sottile, J. Regulation of angiogenesis by extracellular matrix, *Biochimica et biophysica acta* 1654, 13–22 (2004).

85. Simon-Assmann, P. Orend, G. Mammadova-Bach, E. Spenlé, C. & Lefebvre, O. Role of laminins in physiological and pathological angiogenesis, *The International journal of developmental biology* 55, 455–465 (2011).

86. Grant, D. S. *et al.* Interaction of endothelial cells with a laminin A chain peptide (SIKVAV) in vitro and induction of angiogenic behavior in vivo, *Journal of cellular physiology* 153, 614–625 (1992).

87. Schnaper, H. W. Kleinman, H. K. & Grant, D. S. Role of laminin in endothelial cell recognition and differentiation, *Kidney international* 43, 20–25 (1993).

88. Campbell, I. D. & Humphries, M. J. Integrin structure, activation, and interactions, *Cold Spring Harbor perspectives in biology* 3 (2011).

89. Friedland, J. C. Lee, M. H. & Boettiger, D. Mechanically activated integrin switch controls alpha5beta1 function, *Science (New York, N.Y.)* 323, 642–644 (2009).

90. Mavria, G. *et al.* ERK-MAPK signaling opposes Rho-kinase to promote endothelial cell survival and sprouting during angiogenesis, *Cancer cell* 9, 33–44 (2006).

91. Kovács, M. Tóth, J. Hetényi, C. Málnási-Csizmadia, A. & Sellers, J. R. Mechanism of blebbistatin inhibition of myosin II, *The Journal of biological chemistry* 279, 35557–35563 (2004).

92. Connolly, J. O. Simpson, N. Hewlett, L. & Hall, A. Rac regulates endothelial morphogenesis and capillary assembly, *Molecular Biology of the Cell* 13, 2474–2485 (2002).

93. Folkman, J. Role of angiogenesis in tumor growth and metastasis, *Seminars in Oncology* 29, 15–18 (2002).

94. Martins, G. G. & Kolega, J. Endothelial cell protrusion and migration in three-dimensional collagen matrices, *Cell motility and the cytoskeleton* 63, 101–115 (2006).

95. Hakkinen, K. M. Harunaga, J. S. Doyle, A. D. & Yamada, K. M. Direct comparisons of the morphology, migration, cell adhesions, and actin cytoskeleton of fibroblasts in four different three-dimensional extracellular matrices, *Tissue engineering. Part A* 17, 713–724 (2011).

96. van Goethem, E. Poincloux, R. Gauffre, F. Maridonneau-Parini, I. & Le Cabec, V. Matrix architecture dictates three-dimensional migration modes of human macrophages: differential involvement of proteases and podosome-like structures, *Journal of immunology (Baltimore, Md. : 1950)* 184, 1049–1061 (2010).

97. Ghibaudo, M. Di Meglio, J.-M. Hersen, P. & Ladoux, B. Mechanics of cell spreading within 3D-micropatterned environments, *Lab on a chip* 11, 805–812 (2011).

98. Panková, K. Rösel, D. Novotný, M. & Brábek, J. The molecular mechanisms of transition between mesenchymal and amoeboid invasiveness in tumor cells, *Cellular and molecular life sciences : CMLS* 67, 63–71 (2010).

99. Norman, L. L. *et al.* Cell blebbing and membrane area homeostasis in spreading and retracting cells, *Biophysical journal* 99, 1726–1733 (2010).

100. Harada, T. *et al.* Nuclear lamin stiffness is a barrier to 3D migration, but softness can limit survival, *The Journal of cell biology* 204, 669–682 (2014).

101. Sowa, G. A. *et al.* Alterations in gene expression in response to compression of nucleus pulposus cells, *The spine journal : official journal of the North American Spine Society* 11, 36–43 (2011).

102. Liu, Y.-J. *et al.* Confinement and low adhesion induce fast amoeboid migration of slow mesenchymal cells, *Cell* 160, 659–672 (2015).

103. Ruprecht, V. *et al.* Cortical contractility triggers a stochastic switch to fast amoeboid cell motility, *Cell* 160, 673–685 (2015).

104. Kolega, J. The role of myosin II motor activity in distributing myosin asymmetrically and coupling protrusive activity to cell translocation, *Mol. Biol. Cell* 17, 4435–4445 (2006).

105. Li, J. *et al.* Regulation of vascular endothelial cell polarization and migration by Hsp70/Hsp90-organizing protein, *PLoS ONE* 7, e36389 (2012).

106. Maes, H. *et al.* BNIP3 supports melanoma cell migration and vasculogenic mimicry by orchestrating the actin cytoskeleton, *Cell Death Dis* 5, e1127 (2014).

107. Pullar, C. E. *et al.* beta4 integrin and epidermal growth factor coordinately regulate electric field-mediated directional migration via Rac1, *Mol. Biol. Cell* 17, 4925–4935 (2006).

108. Vorotnikov, A. V. & Tyurin-Kuzmin, P. A. Chemotactic signaling in mesenchymal cells compared to amoeboid cells, *Genes & Diseases* 1, 162–173 (2014).

109. Lu, P. Takai, K. Weaver, V. M. & Werb, Z. Extracellular matrix degradation and remodeling in development and disease, *Cold Spring Harbor perspectives in biology* 3 (2011).

110. Page-McCaw, A. Ewald, A. J. & Werb, Z. Matrix metalloproteinases and the regulation of tissue remodelling, *Nature reviews. Molecular cell biology* 8, 221–233 (2007).

111. Schmick, M. & Bastiaens, Philippe I H. The interdependence of membrane shape and cellular signal processing, *Cell* 156, 1132–1138 (2014).

112. Estrach, S. *et al.* Laminin-binding integrins induce Dll4 expression and Notch signaling in endothelial cells, *Circulation research* 109, 172–182 (2011).

113. Stenzel, D. *et al.* Endothelial basement membrane limits tip cell formation by inducing Dll4/Notch signalling in vivo, *EMBO reports* 12, 1135–1143 (2011).

114. Swindle-Reilly, K. E. *et al.* The impact of laminin on 3D neurite extension in collagen gels, *Journal of neural engineering* 9, 46007 (2012).

115. Motoike, T. *et al.* Universal GFP reporter for the study of vascular development, *The Journal of Genetics and Development* 28, 75–81 (2000).

116. Lawson, N. D. & Weinstein, B. M. In Vivo Imaging of Embryonic Vascular Development Using Transgenic Zebrafish, *Developmental Biology* 248, 307–318 (2002).

117. Cross, L. M. Cook, M. A. Lin, S. Chen, J.-N. & Rubinstein, A. L. Rapid analysis of angiogenesis drugs in a live fluorescent zebrafish assay, *Arteriosclerosis, thrombosis, and vascular biology* 23, 911–912 (2003).

118. Bentley, K. Philippides, A. & Ravasz Regan, E. Do endothelial cells dream of eclectic shape?, *Developmental cell* 29, 146–158 (2014).

7 APPENDIX

7 APPENDIX

7.1 Material

7.1.1 General equipment and chemicals

Table 1 General lab equipment and consumables

Equipment	**Manufacturer**
Digital UV Ozone System	Novascan, Ames, USA
Eppendorf Easypet	Eppendorf, Hamburg, Germany
Eppendorf Research Plus 10, 100, 1000 µl	Eppendorf, Hamburg, Germany
HERACell 150i incubator	Thermo Scientific, Bonn, Germany
Incubator	Memmert, Schwabach, Germany
Laminarflow Heraeus, Herasafe	Thermo Scientific, Bonn, Germany
Macrorheometer MCR 302	Anton Paar, Graz, Austria
Megafuge 1.0 RS	Thermo Scientific, Bonn, Germany
Mikro 220R	Hettich, Bäch, Switzerland
Small Vacuum Pump MVP	Novocontrol Tech., Montabaur, Germany
Spin Coater SCC-200	Novocontrol Tech., Montabaur, Germany
Transferpette 20 µl	Brand, Wertheim, Germany
Ultrasonic cleaner	Gallay, Mulgrave, AU
UV-light	Benda, Wiesloch, Germany
ViCell^{TM} XR	Beckman Coulter, Brea, USA
Glass coverslips 24 x 24 mm	VWR, Radnor, USA
Round glass coverslips 25 mm	VWR, Radnor, USA

Table 2 Chemicals

Chemicals	**Manufacturer**
3-aminopropyltriethoxysilane	Sigma Aldrich, St. Louis, USA
Acrylamide solution 40%	Biorad, Munich, Germany
Alpha integrin blocking and IHC kit	Millipore, Darmstadt, Germany
Ammonium persulfate (APS)	Roth, Karlsruhe, Germany
Bis-acrylamide 2%	Biorad, CA, USA
Bovine serum albumin	Sigma Aldrich, St. Louis, USA
Dichlordimethylsilane	Sigma Aldrich, St. Louis, USA
Dimethylsulfoxide	Applichem, Darmstadt, Germany

FluorSave™ Reagent mounting medium	Millipore, Darmstadt, Germany
Glutaraldehyde	Amresco, Solon, USA
HEPES (>99.5%)	Sigma Aldrich, St. Louis, USA
Paraformaldehyde	Applichem, Darmstadt, Germany
Sodium bicarbonate 7.5 %	Sigma Aldrich, St. Louis, USA
Sulfo-SANPAH	Thermo Scientific, Bonn, Germany
Tetramethylene-diamine (TEMED)	Roth, Karlsruhe, Germany
Triton X-100	Roth, Karlsruhe, Germany
Yellow-green microbeads 1 µm, 2% solids	Life Technologies, Carlsbad, USA

7.1.2 Microscope equipment and consumables

Table 3 Microscope equipment and consumables

Equipment and consumables	**Manufacturer**
µ-Slide 8 well, ibiTreat	Ibidi, Martinsried, Germany
µ-Slide 8 well, uncoated	Ibidi, Martinsried, Germany
µ-Slide angiogenesis, ibiTreat	Ibidi, Martinsried, Germany
µ-Slide chemotaxis 3D, ibiTreat	Ibidi, Martinsried, Germany
µ-Slide VI 0.4, ibiTreat	Ibidi, Martinsried, Germany
CCD camera DS-Qi1Mc	Nikon, Duesseldorf, Germany
Cover slips 8 well (8 x 8 x 0.17 mm)	H.Saur Laborbedarf, Reutlingen, Germany
Gas incubation system	Ibidi, Martinsried, Germany
Heating system	Okolab, Pozzuoli, Italy
Heating system, multi-well plates	Ibidi, Martinsried, Germany
Heating system, universal fit	Ibidi, Martinsried, Germany
Inverted microscope Eclipse Ti	Nikon, Duesseldorf, Germany
Plan Apochromat 63x/1.2 NA water objective	Leica, Wetzlar, Germany
Plan Apochromat 63x/1.3 NA glycerol objective	Leica, Wetzlar, Germany
Plan Apochromat 63x/1.4 NA oil objective	Leica, Wetzlar, Germany
TCS SP8 SMD	Leica, Wetzlar, Germany

7.1.3 Cell culture consumables

Table 4 Cell culture consumables

Consumables	**Manufacturer**
10x endothelial cell basal medium	PromoCell, Heidelberg, Germany
Amphotericin B 250 µg/ml	AppliChem, Darmstadt, Germany
Collagen G	Biochrom AG, Berlin, Germany
Collagenase A	Roche, Mannheim, Germany
Dulbecco's modified Eagle's medium (DMEM)	PAN-Biotech, Aidenbach, Germany
EDTA disodium salt dihydrate	Roth, Karlsruhe, Germany
Endothelial cell growth medium kit enhanced	PELOBiotech, Martinsried, Germany
Endothelial cell growth medium with Supplement Mix C-39215	PromoCell, Heidelberg, Germany
Fetal calf serum	PAA Laboratories, Pasching, Austria
M199 medium	PAN-Biotech, Aidenbach, Germany
Penicillin/Streptomycin 10 000 U/ml	PAN-Biotech, Aidenbach, Germany
Sodium bicarbonate	Sigma Aldrich, St. Louis, USA
Targefect-HUVEC kit	Targetingsystems, El Cajon, USA
Trypsin	PAN-Biotech, Aidenbach, Germany

7.1.4 Inhibitors

Table 5 Pharmacological inhibitors

Inhibitor	**Manufacturer**
Batimastat	Sigma Aldrich, St. Louis, USA
Blebbistatin	Sigma Aldrich, St. Louis, USA
ML141	Sigma Aldrich, St. Louis, USA
Rac1 inhibitor 553502	Millipore, Darmstadt, Germany
Y27632	Sigma Aldrich, St. Louis, USA

7.1.5 Antibodies for immunofluorescence

Table 6 Primary and secondary antibodies

Primary or secondary antibody	**Manufacturer**
Alexa Fluor 488, donkey anti-rat, IgG (H+L)	Life Technologies, Carlsbad, USA
Alexa Fluor 488, goat anti-mouse, IgG (H+L)	Life Technologies, Carlsbad, USA
Alexa Fluor 488, goat anti-rabbit, IgG (H+L)	Life Technologies, Carlsbad, USA
Alexa Fluor 680, goat anti-mouse, IgG (H+L)	Life Technologies, Carlsbad, USA
Alexa Fluor 680, goat anti-rabbit, IgG (H+L)	Life Technologies, Carlsbad, USA
Alexa Fluor 680, goat, anti-rat, IgG (H+L)	Life Technologies, Carlsbad, USA
Cdc42, rabbit, pAb	Santa Cruz, Heidelberg, Germany
Collagen type I, mouse, mAb	Sigma Aldrich, St. Louis, USA
Collagen type I, rabbit, pAb	Abcam, Cambridge, UK
Collagen type IV, rabbit, pAb	Millipore, Darmstadt, Germany
Entactin, rat, mAb	Santa Cruz, Heidelberg, Germany
Fibronectin, mouse, mAb	Santa Cruz, Heidelberg, Germany
Laminin, rabbit, pAb	Sigma Aldrich, St. Louis, USA
Rac1, mouse, mAb	Thermo Scientific, Bonn, Germany

7.1.6 Fluorescent dyes

Table 7 Fluorescent dyes

Fluorescent dye	**Manufacturer**
Hoechst 33342	Sigma Aldrich, St. Louis, USA
Isolectin GS-B_4,Alexa 488 conjugate	Life Technologies, Carlsbad, USA
Rhodamine phalloidin	Life Technologies, Carlsbad, USA

7.1.7 Hydrogels

Table 8 Natural hydrogels

Hydrogel	**Manufacturer**
Collagen type I, rat tail, 5 mg/ml, non-pepsinized	Ibidi, Martinsried, Germany
Matrigel, growth factor reduced, phenol red free	Corning, Amsterdam, Netherlands

7.1.8 Buffers

Table 9 Buffers

Solution	**Composition**
PBS (pH 7.4)	123.3 mM NaCl 10.4 mM Na_2HPO_4 3.2 mM KH_2PO_4 in H_2O
PBS + Ca^{2+}/Mg^{2+} (pH 7.4)	136.9 mM NaCl 2.7 mM KCl 8.1 mM Na_2HPO_4 1.5 mM KH_2PO_4 0.5 mM $MgCl_2$ x 6 H_2O 0.7 mM $CaCl_2$ x 2 H_2O in H_2O
Retina blocking buffer	0.5 ml 1% BSA 0.3% Triton X-100 50 ml PBS (pH 7.4)
PBlec	1 mM $MgCl_2$ 1 mM $CaCl_2$ $MnCl_2$ 10% Triton X-100 50 ml PBS (pH 7.4)

7.2 Simulation parameters

Table 10 Parameters for simulation of endothelial tube formation

A	Energy gain per created contact
a_α	Area
B	Energy loss per broken contact
D	Diffusion coefficient
d_{max}	Maximum strand length
m_α	Marker
Q_α	Upper polarization bound
q_α	Lower polarization bound
r_α	Velocity of cytoskeleton-adaption
$R_{\alpha/\beta}$	Diffusion speed of chemical signals within cells α or β
α	Secretion rate of the chemoattractant
γ	Decay rate of the chemoattractant
K	Force with which cells respond to the chemotactic gradient
λ	Increase of anchoring sites along strands

7.3 Publications

7.3.1 Original publications

Spatio-temporal characterization of endothelial tube formation: Early stages of morphogenesis are driven by mechanotransduction
Kerstin Kick, Andriy Goychuk, Berenice Jahn, Carina Wollnik, Florian Rehfeldt, Angelika M. Vollmar, Erwin Frey, Stefan Zahler
In preparation

A new view on endothelial cell migration: Switching of migration modes based on matrix composition
Kerstin Kick, Katharina Nekolla, Markus Rehberg, Angelika M. Vollmar, Stefan Zahler
In preparation

Morphological switching of endothelial cells on micro-tracks mimics aspects of 3D migration in collagen gels
Simon L. Schuster, Felix J. Segerer, Kerstin Kick, Florian A. Gegenfurtner, Christoph Schreiber, Max Albert, Angelika M. Vollmar, Joachim O. Rädler, Stefan Zahler
In preparation

Influence of surface modifications on the spatio-temporal microdistribution of quantum dots in *vivo*
Katharina Nekolla, Kerstin Kick, Sabine Sellner, Karina Mildner, Stefan Zahler, Dagmar Zeuschner, Fritz Krombach, Markus Rehberg
In preparation

The biophysical properties of basal lamina gels depend on the biochemical composition of the gel
Fabienna Arends*, Constantin Nowald*, Kerstin Pflieger, Kathrin Boettcher, Stefan Zahler, Oliver Lieleg
PLoS One. 2015 Feb 17; 10(2)

Components of the plasminogen activation system promote engraftment of porous polyethylene biomaterial via common and distinct effects
Christoph A. Reichel*, Maximilian E. T. Hessenauer *, Kerstin Pflieger, Markus Rehberg, Sandip M. Kanse, Stefan Zahler, Fritz Krombach, Alexander Berghaus, Sebastian Strieth

PLoS One. 2015 Feb 6; 10(2)

The impact of cysteine-rich intestinal protein 1 (CRIP1) in human breast cancer
Natalie Ludyga, Sonja Englert, Kerstin Pflieger, Sandra Rauser, Herbert Braselmann, Axel Walch, Gert Auer, Heinz Höfler, Michaela Aubele
Molecular Cancer. 2013; 12:28

*These authors contribute equally.

7.3.2 Poster presentations

Endothelial cell migration in three-dimensional hydrogels - focusing on angiogenesis
Kerstin Pflieger, Angelika M. Vollmar, Stefan Zahler
SFB 1032 Retreat 2015, February 3-5, Altoetting, Germany

Endothelial cell migration in three-dimensional hydrogels - focusing on angiogenesis
Kerstin Pflieger, Angelika M. Vollmar, Stefan Zahler
American Society for Matrix Biology (ASMB) Biennial Meeting 2014, October 12-15, Cleveland, Ohio

Characterization of HUVEC migration in hydrogels focusing on angiogenesis
Kerstin Pflieger, Stefan Zahler
International Physics of Living Systems Network (iPoLS) 2014, July 21-24, Munich, Germany

Controlling cellular function by structured surfaces: “Artificial angiogenesis”
Kerstin Pflieger, Simon Schuster, Angelika M. Vollmar, Stefan Zahler
SFB 1032 Spring Workshop 2013/ Joint Meeting NIM Areas IV and V 2013, February 18-19, Hohenkammer, Germany

7.3.3 Oral presentations

“Artificial Angiogenesis” – Set the stage for new models
Kerstin Pflieger, Simon Schuster, Stefan Zahler
SFB 1032 Retreat 2014, February 24-25, Frauenchiemsee, Germany

7.4 Curriculum Vitae

Persönliche Daten

Name	Kerstin Kick, geb. Pflieger
Geburtsdatum	25.07.1988
Geburtsort	Deggendorf
Familienstand	verheiratet
Staatsangehörigkeit	deutsch

Ausbildung

ab 10/2012	Dissertation am Lehrstuhl für Pharmazeutische Biologie Department Pharmazie der LMU München Betreuer: Prof. Dr. Stefan Zahler
10/2010-10/2012	Studium der Biochemie (Master of Science) Technische Universität München
10/2007-09/2010	Studium der Biochemie (Bachelor of Science) Technische Universität München
06/2007	Abitur Robert-Koch-Gymnasium Deggendorf

7.5 Danksagung

An erster Stelle möchte ich mich bei Frau Prof. Vollmar und Herrn Prof. Zahler dafür bedanken, dass Sie mir diese Promotion ermöglicht haben.

Herr Zahler, vielen Dank, für Ihr Vertrauen in meine Arbeit, für die schöpferische Freiheit, die Sie mir bei der Bearbeitung des Themas gegeben haben und für Ihre Unterstützung, wenn ich sie gebraucht habe.

Ein weiterer Dank geht an Herrn PD Rehberg, Herrn Prof. Frieß, Herrn PD Michalakis und Herrn Prof. Wahl-Schott. Vielen Dank, dass Sie sich die Zeit genommen haben, Teil meines Prüfungskomitees zu sein.

Außerdem möchte ich mich bei meinen Kooperationspartnern für die hervorragende Zusammenarbeit bedanken: Herrn Prof. Frey und Andriy Goychuk, für die interessanten Gespräche und Einblicke in die theoretische Physik, und Markus Rehberg und Katharina Nekolla, für die Unterstützung in allen Belangen. Danke!

Ein besonderer Dank geht auch an den Sonderforschungsbereich 1032, der diese Arbeit finanziert hat. Vielen Dank, vor allem Marilena Pinto, für die außergewöhnlich gute Unterstützung und Förderung der Doktoranden, und für die hervorragend organisierten Workshops und Seminare.

In diesem Zuge möchte ich mich auch ganz herzlich bei den anderen „SFB Doktoranden“, vor allem bei Katharina, Sabine, Christoph und Felix, für die gute Zusammenarbeit und die super Stimmung bei allen SFB-Aktivitäten bedanken. Es war schön im Rahmen des Graduiertenkollegs so viele nette Menschen kenngelernt zu haben.

Mein größter Dank geht auch an alle aktuellen und ehemaligen Mitarbeiter des AK Vollmars. Es war schön ein Teil dieser Gruppe zu sein. Besonders möchte ich mich bei meinen aktuellen Labor- und Teamkollegen Lisa, Flo und Simon bedanken: Danke, für das gute Laborklima und den Zusammenhalt!

Besonders bedanken möchte ich mich bei Jana und Kerstin. Vielen Dank euch beiden für eure tägliche Unterstützung im Labor, aber auch für die vielen persönlichen Gespräche. Danke Kerstin, für die schöne Zeit. Danke Jana, dass du immer ein offenes Ohr für mich hattest und, dass du dich immer so herzlich um mich gekümmert hast.

Melli und Andi, euch Danke ich dafür, dass es euch gibt und, dass ich mich immer auf euch verlassen kann. Schön, solche Freunde zu haben.

Ich möchte mich von Herzen bei meinen Eltern bedanken. Mama, Papa danke, dass ihr immer an mich geglaubt habt. Eure Unterstützung und Liebe war immer meine größte Motivation. Danke!

Mein größter Dank geht an den wichtigsten Menschen in meinem Leben. Lieber Benjamin, vielen Dank, dass du immer für mich da bist, und jeden Tag meines Lebens so besonders machst!